AD-A267 167

NAVAL POSTGRADUATE SCHOOL
Monterey, California

DTIC
ELECTE
JUL 27 1993
S B D

THESIS

THE THREE-DIMENSIONAL RAY TRAJECTORIES
OF THE WKB OPTICAL FIBER MODES

by

Athanasios Nassopoulos

March, 1993

Thesis Advisor: Ronald J. Pieper

Approved for public release; distribution is unlimited.

93-16824

Unclassified

Security Classification of this page

REPORT DOCUMENTATION PAGE

1a Report Security Classification: Unclassified			1b Restrictive Markings	
2a Security Classification Authority			3 Distribution/Availability of Report	
2b Declassification/Downgrading Schedule			Approved for public release; distribution is unlimited.	
4 Performing Organization Report Number(s)			5 Monitoring Organization Report Number(s)	
6a Name of Performing Organization Naval Postgraduate School	6b Office Symbol *(if applicable)* EC		7a Name of Monitoring Organization Naval Postgraduate School	
6c Address *(city, state, and ZIP code)* Monterey CA 93943-5000			7b Address *(city, state, and ZIP code)* Monterey CA 93943-5000	
8a Name of Funding/Sponsoring Organization	6b Office Symbol *(if applicable)*		9 Procurement Instrument Identification Number	
Address *(city, state, and ZIP code)*			10 Source of Funding Numbers	
			Program Element No / Project No / Task No / Work Unit Accession No	
11 Title *(include security classification)* THE THREE-DIMENSIONAL RAY TRAJECTORIES OF THE WKB FIBER OPTICS				
12 Personal Author(s) Athanasios Nassopoulos				
13a Type of Report Master's Thesis	13b Time Covered From To		14 Date of Report *(year, month, day)* March 1993	15 Page Count 103
16 Supplementary Notation The views expressed in this thesis are those of the author and do not reflect the official policy or position of the Department of Defense or the U.S. Government.				
17 Cosati Codes			18 Subject Terms *(continue on reverse if necessary and identify by block number)*	
Field / Group / Subgroup			optical fibers, waveguide mode numbers, ray trajectories	

19 Abstract *(continue on reverse if necessary and identify by block number)*

A model that produces three-dimensional ray trajectories in an optical fiber is derived through the use of a simple correspondence rule. The analysis and simulations presented will be in terms of dimensionless parameters. The curves prepared ar presented for allowed radial and azimuthal mode numbers and are presented in terms of dimensions which are normalized by the core radius. The model presented will be shown to be in agreement with the standard Eikonal ray theory and will serve as a link between the ray trajectories and the mode numbers of the WKB waveguide solutions of an optical fiber.

20 Distribution/Availability of Abstract _X unclassified/unlimited __ same as report __ DTIC users	21 Abstract Security Classification Unclassified	
22a Name of Responsible Individual Ronald J. Pieper	22b Telephone *(include Area Code)* (408) 646-2101	22c Office Symbol EC/Pr

DD FORM 1473,84 MAR 83 APR edition may be used until exhausted

All other editions are obsolete

security classification of this page

Unclassified

Approved for public release; distribution is unlimited.

THE THREE-DIMENSIONAL RAY TRAJECTORIES OF THE WKB OPTICAL FIBER MODES

by

Athanasios Nassopoulos
Lieutenant Junior Grade, Hellenic Navy
B.S., Hellenic Naval Academy, 1984

Submitted in partial fulfillment
of the requirements for the degree of

MASTER OF SCIENCE IN ELECTRICAL ENGINEERING

from the

NAVAL POSTGRADUATE SCHOOL
March, 1993

Author: _____
Athanasios Nassopoulos

Approved by: _____
Ronald J. Pieper, Thesis Advisor

_____
Lawrence J. Ziomek, Second Reader

_____
Michael A. Morgan, Chairman
Department of Electrical and Computer Engineering

ABSTRACT

A model that produces three-dimensional ray trajectories in an optical fiber is derived through the use of a simple correspondence rule. The analysis and simulations presented will be in terms of dimensionless parameters. The curves prepared are presented for allowed radial and azimuthal mode numbers and are presented in terms of dimensions which are normalized by the core radius. The model presented will be shown to be in agreement with the standard Eikonal ray theory and will serve as a link between the ray trajectories and the mode numbers of the WKB waveguide solutions of an optical fiber.

DTIC COPY INSPECTED 3

Accession For
NTIS GRA&I ☑
DTIC TAB ☐
Unannounced ☐
Justification
By
Distribution/
Availability Codes
Dist | Avail and/or Special
A-1

TABLE OF CONTENTS

LIST OF FIGURES

LIST OF TABLES

I. INTRODUCTION

A. REVIEW OF PRIOR WORK

An extensive body of literature exists for both wave and ray characterization of optical fibers. It is generally accepted that exact waveguide solutions exist for a select number of specific index profiles [Ref. 1, 2]. The exact waveguide solutions are frequently derived for step index fibers in intermediate level optical fiber texts. For example, Cherin's Optical Fiber Communications [Ref. 3] provides a fairly clear waveguide analysis of the step index fiber. In the general case of graded index fibers the problem is not analytically tractable without approximation [Ref. 1]. The most common technique for the analysis of graded index fibers is based on the WKB approximation [Ref. 4, 5, 6, 7]. It is possible to show that the first-order WKB approximation is equivalent to the results produced from a simple ray model [Ref. 8].

Despite the mathematical importance of having an exact solution for the waveguide fibers in an optical fiber, the propagation characteristics can be difficult to visualize. It is not surprising that an alternative approach to treating optical fibers, based on the Eikonal ray approach [Ref. 9, 10, 11, 12], which in turn is based on Fermat's extremum principle

[Ref. 10, 11, 12, 13, 14], has proven to be extremely useful in explaining effects which take place in optical fibers. For example, application of such techniques to the prediction of bending losses in optical fibers has appeared in the literature [Ref. 13, 15]. In addition, achromatic modal dispersion effects have been predicted with ray models [Ref. 16]. It has been shown that the exact step index radical function has a first inflection point at the inner ray caustic or turning point [Ref. 8]. To a significant degree the association between the WKB wave solutions, which depends on azimuthal and radial mode numbers, and ray models has not been fully explored. For example, the ray trajectories were typically derived for arbitrary initial conditions without regard for ray conditions dictated by invariant conditions associated with mode specific quantum numbers.

Recently, an approach based on a simple correspondence between waves and rays has been proposed [Ref. 17] as a substitute for the first-order WKB approach of counting modes [Ref. 9]. This correspondence principle has been used to qualitatively demonstrate that there should be a direct association between the mode numbers in an optical fiber and the ray trajectories. The main focus of this thesis is to treat this association quantitatively.

B. OBJECTIVES OF THE THESIS

The correspondence principle [Ref. 17] leads to rules which predict both initial conditions and propagator conditions on ray trajectories associated with specific modes. This thesis will cover all background analysis leading to application of these rules to meridional rays and skew rays in a graded index fiber. Whenever necessary for visualization, full three-dimensional ray trajectories are provided. The analysis and program simulations are derived and implemented, respectively, in a normalized form with respect to the vacuum wavelength and core radius. As a result, the computer results are generalized to a broader class of problems. Specifically, the optical fiber rays are expressed in terms of the commonly used V-parameter, numerical aperture and core index. Appendix B has been dedicated to demonstrating that the correspondence principle, mentioned above, leads to propagator conditions which are precisely equivalent to rules obtained from the standard Eikonal model. Appendix A has outlined in flowchart fashion the conceptional development of the programs. Appendix E of the thesis manuscript has been scheduled for an IEEE publication [Ref. 19] in March 1993.

C. OVERVIEW OF THE THESIS

Chapter I is the introduction and covers both a review of relevant literature and a thesis overview. In the interest of keeping this thesis fairly self-contained, Chapter II provides

a brief technical description of essential background preliminaries.

In Chapter III, the basis for the specific problems examined in later chapters is provided. A conceptual flowchart shown in Appendix A summarizes the basic analysis which leads to mode specific trajectories.

In Chapter IV, attention is given to meridional rays for the arbitrary α profile. The specific meridional ray cases of step index fibers ($\alpha=\infty$) and parabolicity ($\alpha=2$) are both analyzed in detail. Appendix D provides a useful mathematical analysis for the essential function $F(\alpha)$, a normalization integral used in this chapter.

In Chapter V, the solutions for the step index skew rays are obtained. This chapter is a link between the general formulation of Chapter III and the more complete step index analysis contained in Appendix E.

In Chapter VI, numerical solutions for skew rays with arbitrary α profile is provided. Some useful variations of fiber optic parameters due to initial conditions are also demonstrated and explained here.

In Chapter VII, quasi analytic solutions for the interesting case of skew rays with $\alpha=2$ are presented. The well known fact of the orbital periodicity of this case is also proven here.

Appendix B shows the exact agreement between the ray analysis presented and the Eikonal analysis.

Appendix C provides a symbol table which contains notation for the most common symbols used throughout in the thesis.

II. BACKGROUND

Starting from the Hemholtz equation, which is the phasor form of the linear wave equation for isotropic, source-free, homogeneous media, we have

$$[\nabla^2+k^2(\vec{r})]\vec{E}=0, \tag{2-1}$$

where $k(\vec{r})$ is the wave number and $\vec{E}$ is the electric field. It is noted that this equation is only approximately valid in a graded index fiber. Consistent with the form given in (2-1), we assume that

$$k(\vec{r})=n(\vec{r})\,k=k_r\hat{e}_r+k_\phi\hat{e}_\phi+k_z\hat{e}_z, \tag{2-2}$$

where k is the vacuum wave number, $n(\vec{r})$ is the index of refraction, (r, ϕ, z) are the cylindrical coordinates needed to describe points in the fiber and ($\hat{e}_r$, $\hat{e}_\phi$, $\hat{e}_z$) are the unit vectors of the coordinate system.

We list here the basic assumptions that $n(\vec{r})$ satisfies

1. The index depends on the distance from the symmetry axis of the fiber (viz. $n(\vec{r})=n(r)$).
2. The index is a decreasing function for $r\le a$.
3. The index is constant for $r\ge a$.

These restrictions can be represented in Figure 1 where $k(r)=kn(r)$.

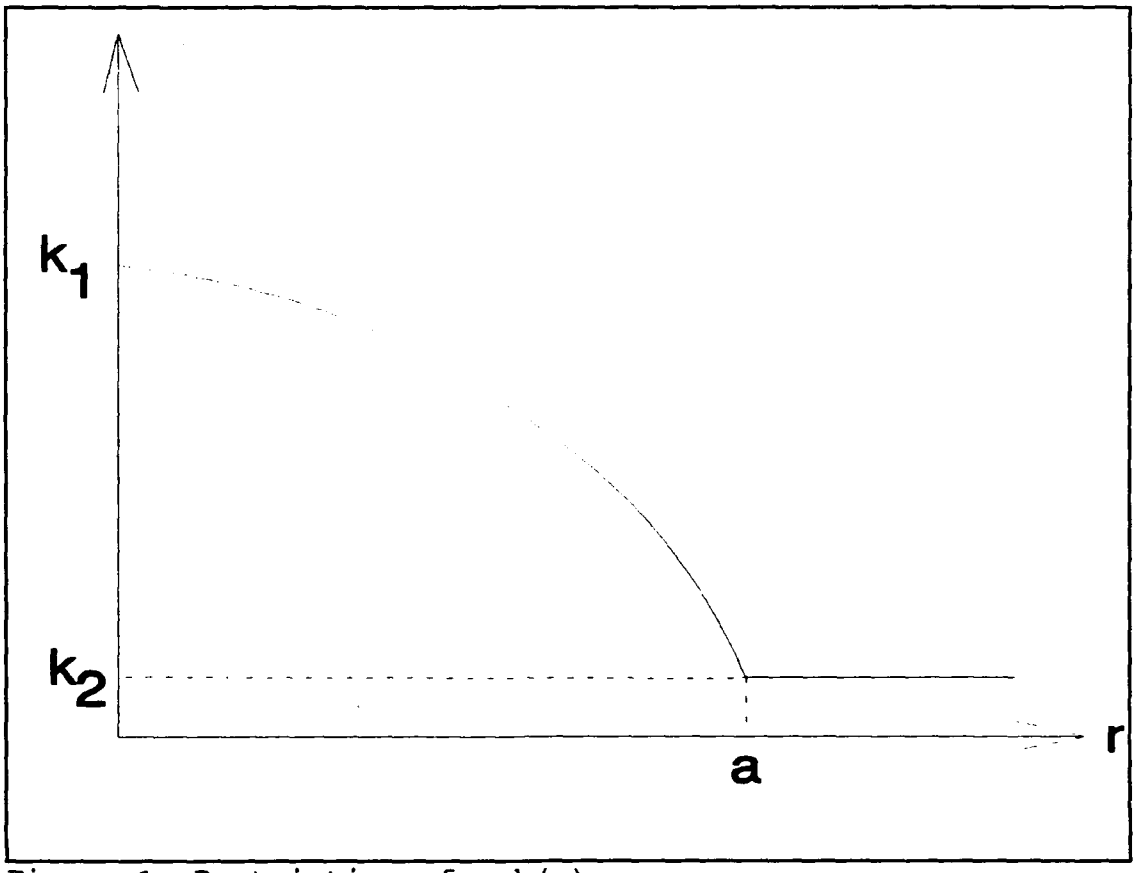

Figure 1: Restrictions for k(r).

Following a standard procedure [Ref. 1] in waveguide analysis, we assume that the general phasor for the z component of the electric field in the cylindrical optical fiber can be represented as

$$E_z(r) = F_\nu(r)\, e^{j\nu\phi} e^{-j\beta z}, \qquad (2\text{-}3)$$

where $F_\nu(r)$ is the radial solution to (2-1), β is the phase constant of the waveguide, and ν is the azimuthal mode number, which is forced to be an integer due to periodic boundary conditions [Ref. 1].

In the case of a step index fiber, an application of Maxwell's equations leads to a transcendental equation for the phase constant. The equation has a finite number of discrete solutions for each integer ν [Ref. 1]. The obtained convention for ordering these solutions is

$$\beta_{\nu_1}>\beta_{\nu_2}\ldots>\beta_{\nu_m}>\beta_{\nu_{m+1}}, \tag{2-4}$$

where the second subscript m is known as the radial mode number. This convention is also applied to the approximate WKB [Ref. 7] solutions in inhomogeneous optical fibers.

A simple correspondence rule for plane waves [Ref. 17]

$$\vec{\nabla}=-j\vec{k}, \tag{2-5}$$

can be applied to the ϕ and z dependencies of (2-3). The grad operator is given by [Ref. 18]

$$\vec{\nabla}=\hat{e}_r\frac{\partial}{\partial r}+\hat{e}_\phi\frac{1}{r}\frac{\partial}{\partial\phi}+\hat{e}_z\frac{\partial}{\partial z}. \tag{2-6}$$

It now follows from (2-6) and (2-3) that

$$j(\vec{\nabla}E_z)_\phi=j\frac{\nu}{r}E_z, \tag{2-7}$$

which from (2-5) leads to

$$k_\phi=-\frac{\nu}{r}. \tag{2-8}$$

Similarly,

$$j(\vec{\nabla}E_z)_z=-j\beta E_z, \tag{2-9}$$

and again from (2-5)

$$k_z=\beta. \tag{2-10}$$

It is noted from (2-3) that the correspondence rule applies only to the ϕ and z components.

Using the relation between the propagation vector and its components, it follows from (2-2), (2-8) and (2-10) that the radial component of the propagation vector can be expressed as

$$k_r=\pm\sqrt{k^2(r)-\beta^2-(\frac{\nu}{r})^2}\,. \tag{2-11}$$

Both + and - roots are required for the development of a full cycle of a trajectory. Nevertheless, symmetry conditions in the trajectory will allow the analysis to be based on the + root only. Furthermore, for k_r to correspond to a bounded orbit, it must be real [Ref. 1, 8]. Without loss in generality, we can continue with only the + form for k_r. According to (2-4) and (2-11), the radial component of the propagation vector will increase with increasing m (see Figure 2). The crosshatched domain of Figure 3 represents the condition that k_r is real. Therefore, terms under the radical of (2-11) satisfy

$$k_r^2=k^2(r)-\beta^2-(\frac{\nu}{r})^2\geq 0. \tag{2-12}$$

A condition of phase synchronization [Ref. 1] on the radial part of the wave vector results in the approximate expression

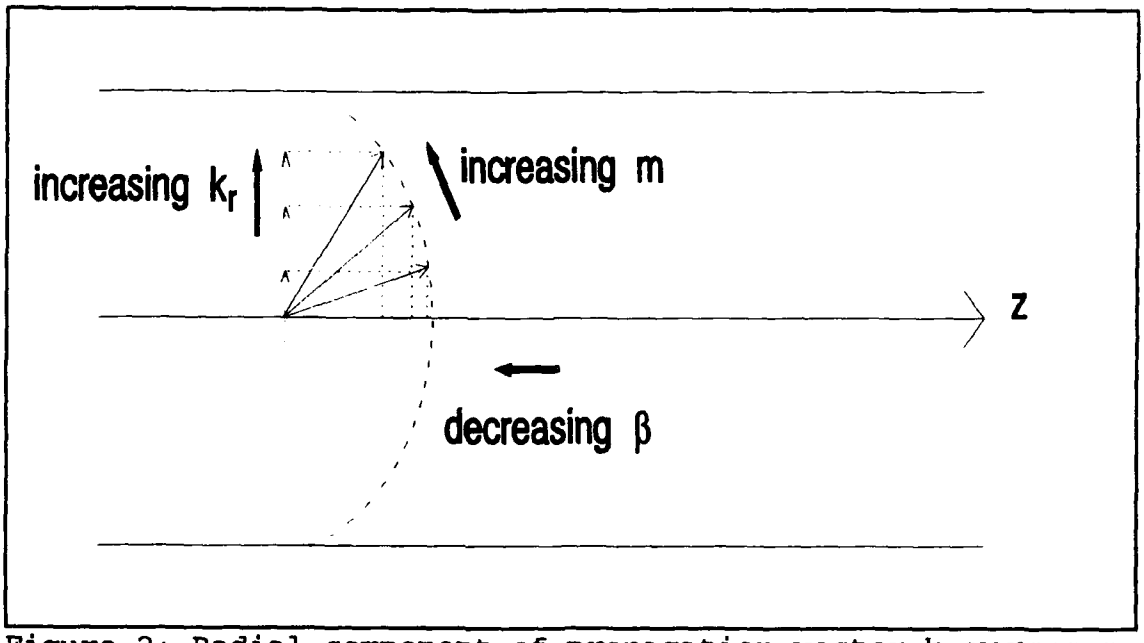

Figure 2: Radial component of propagation vector k_r versus m.

$$m \approx \frac{1}{\pi}\int_{r_1}^{r_2}\sqrt{k^2(r)-\beta^2-(\frac{\nu}{r})^2}\,dr, \qquad (2\text{-}13)$$

where the radial mode number m must take on positive integer values. The integral limits r_1 and r_2, are the two values for which the integrand of (2-13) is zero. These are generally referred to as the turning points as represented in Figure 3. We note that r_1 and r_2 satisfy

$$k_r^2 = k^2(r)-\beta^2-(\frac{\nu}{r})^2 = 0. \qquad (2\text{-}14)$$

More precisely, the relation (2-13) becomes exact after the substitutions $m \to m+\frac{1}{2}$ and $\nu^2 \to \nu^2-\frac{1}{4}$ [Ref. 5]. In the WKB analysis of optical fibers, these offsets are usually ignored.

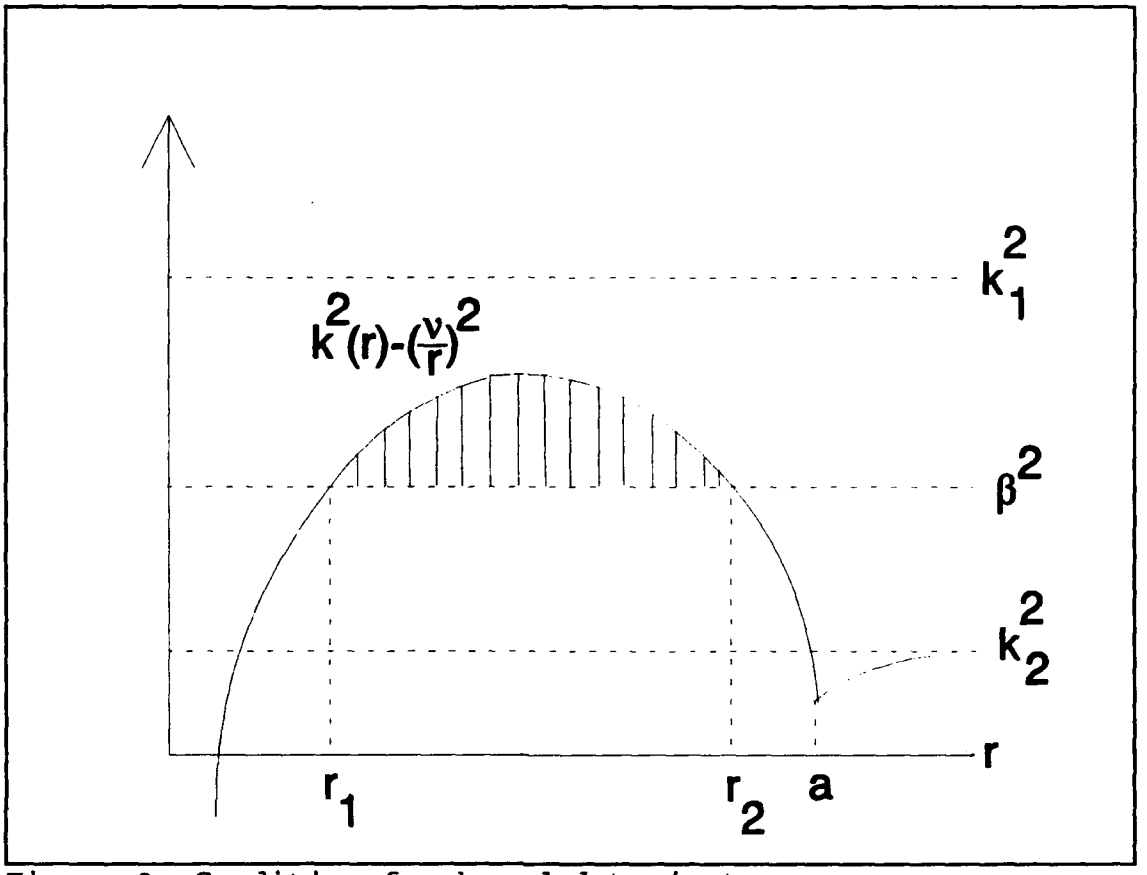

Figure 3: Condition for bounded trajectory.

A significant point relates Figure 3 to the radial mode number given by (2-13). The value of m is qualitatively proportional to the cross-hatched area. The general procedure to find the maximum m is to allow β^2 to be equal to k_2^2. If β^2 falls below k_2^2, then the additional modes created are no longer trapped. Many authors have explored the interpretation that the optical fiber trajectory is equivalent to the trajectory of a particle in a potential well [Ref. 8].

Figure 3 correctly suggests that there is a maximum ν for which the cross-hatched region vanishes. Clearly there is an

upper limit on the value of ν which occurs for the condition $r_1=r_2$. The general relation between the turning points and ν can be obtained from (2-14) as

$$\nu=r\sqrt{k^2(r)-\beta^2}\ , \tag{2-15}$$

which is represented in Figure 4. It is apparent from Figure 3 that the condition $\beta=kn_2$ will allow the maximum range in ν and the corresponding maximum in the peak on Figure 4. In calculating ν_{max}, $\nu(r_p)$ will in general be evaluated under the stated limiting condition $\beta=kn_2$. At $\nu=0$, the solutions for turning points are easily read off in Figure 4 as 0 and $n^{-1}(\frac{\beta}{k})$. Since $\frac{\beta}{k}=n_1\cos\theta$, the second condition leads to the condition for total internal reflection

$$n(r_2)=n_1\cos\theta. \tag{2-16}$$

For the step index fiber, $r_2=a$, which leads to the well known relation

$$\cos\theta=\frac{n_2}{n_1}. \tag{2-17}$$

Equations (2-8), (2-10), (2-11), (2-12) and (2-15) become the basis for the three-dimensional ray modeling that will be the focus of the discussion that follows. It is noted that the components (k_r, k_ϕ, k_z) will describe the direction of the ray and that coordinates (r, ϕ, z) locate the ray. For purposes of

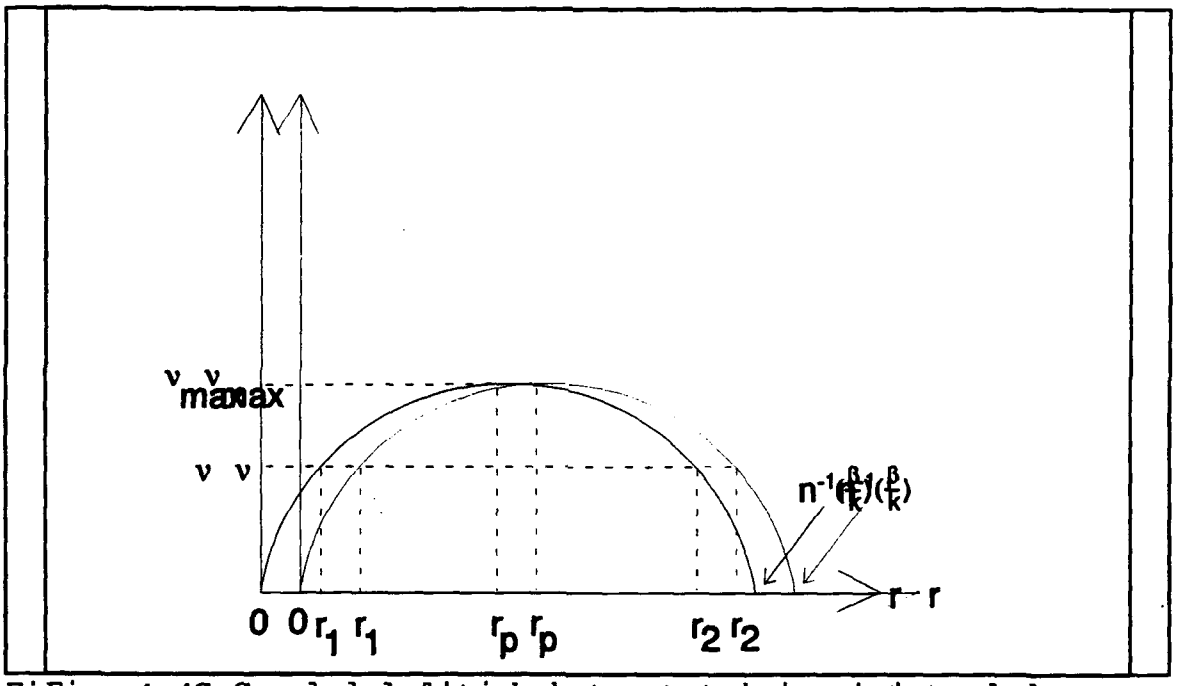

Figure 4: General relation between turning points and ν.

analysis, the geometrical relationships are more carefully defined in the next chapter.

Best Available Copy

III. GENERAL CHARACTERIZATION OF THE THREE-DIMENSIONAL RAY MODEL

A. INTRODUCTORY REMARKS

This chapter will provide a basis for the specific categories of problems examined in later chapters (e.g., meridional, skew step index, and skew graded index). A general approach to the goal of obtaining mode-connected ray trajectories will be presented at the end of the chapter.

B. GEOMETRY OF THE PROBLEM

With reference to Figure 5, the orientation of the wave vector is defined in terms of θ and ξ. It follows that

$$k_\phi = k(r)\sin\theta\ \sin\xi, \tag{3-1}$$

$$k_z = k(r)\cos\theta, \tag{3-2}$$

and

$$k_r = k(r)\sin\theta\ \cos\xi. \tag{3-3}$$

The incremental line variation in the ray trajectory can be defined as

$$\vec{dl} = dz\ \hat{e}_z + dr\ \hat{e}_r + r\ d\phi\ \hat{e}_\phi. \tag{3-4}$$

The propagation vector, defined by the cylindrical components (3-1), (3-2) and (3-3), is perpendicular to the wavefronts of constant phase and therefore tangent to the ray trajectories.

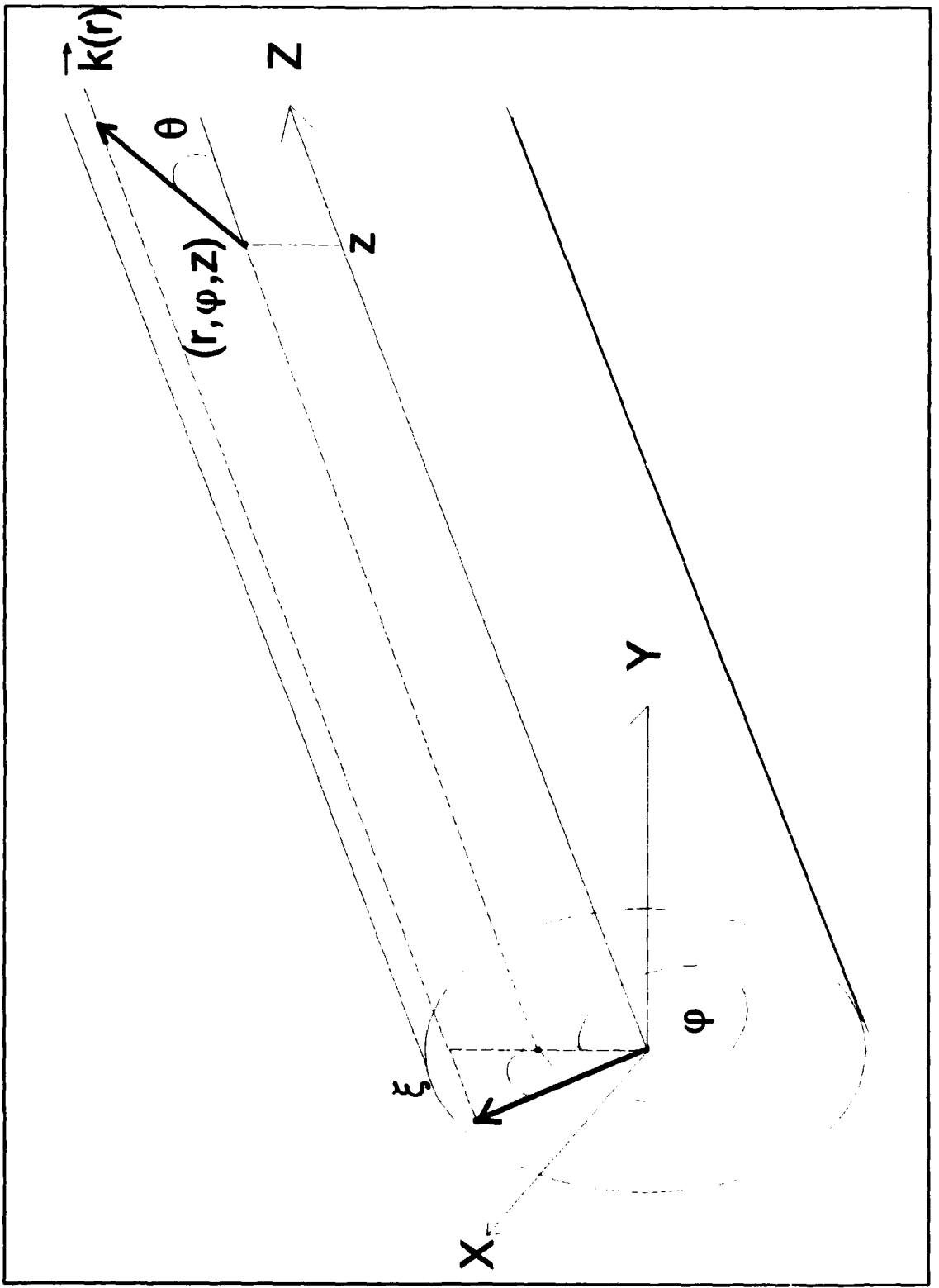

Figure 5: Geometry of the problem.

Therefore, the incremental components $d\phi$, dr, and dz are tangential to (2-8), (2-10) and (2-11), respectively, and it follows

$$dz = dl \cos\theta, \tag{3-5}$$

$$dr = dl \sin\theta \cos\xi \tag{3-6}$$

and

$$r\, d\phi = dl \sin\theta \sin\xi. \tag{3-7}$$

C. MODELING ANALYSIS

1. Computation of the turning points

Without any loss in generality, we assume that the index profile can be expressed in terms of a standard power profile, which is matched to the edge conditions,

$$n(0) = n_1 \tag{3-8}$$

and

$$n(a) = n_2, \tag{3-9}$$

and a perturbation f(r) as shown below

$$k^2 n^2(r) = k^2 [n_p^2(r) + NA^2 f(r)], \tag{3-10}$$

where

$$f(0) = f(a) = 0. \tag{3-11}$$

The numerical aperture of the fiber is given by [Ref. 1]

$$NA=\sqrt{n_1^2-n_2^2} \tag{3-12}$$

and the power profile satisfies

$$n_p^2=n_1^2[1-2\Delta(\frac{r}{a})^{\alpha}], \tag{3-13}$$

in which the index difference for this formula is defined as

$$\Delta=\frac{n_1^2-n_2^2}{2n_1^2}. \tag{3-14}$$

It can be easily checked that at r=a, $n_p=n_2$.

Substitution of (3-12) into (2-12) leads to

$$m=\frac{V}{\pi}\int_{\bar{r}_1}^{\bar{r}_2}\sqrt{\epsilon(\beta)\bar{r}^2+f(r)-(\frac{\nu}{V})^2-\bar{r}^{\alpha+2}}\,\frac{d\bar{r}}{\bar{r}} \tag{3-15}$$

where the V-parameter is given by [Ref. 1]

$$V=kNAa, \tag{3-16}$$

the normalized phase constant, $\epsilon(\beta)$, is defined by

$$\epsilon(\beta)=\frac{n_1^2-(\frac{\beta}{k})^2}{NA^2} \tag{3-17}$$

and

(3-18)

defines the radial normalization.

In order to further analyze the problem, the perturbation of the index power will be dropped. After taking f(r)=0, the condition on the turning points will satisfy

$$\bar{r}^{\alpha+2}-\epsilon(\beta)\bar{r}^2+(\frac{\nu}{V})^2=0, \qquad (3\text{-}19)$$

which is a normalized version of condition (2-14). Figure 6 is plotted for α=2, V=100, ν=10 and $\epsilon(\beta)$ as stated on the Figure. It is noted that as $\epsilon(\beta)$ increases, the zero crossing points (or turning points) should move closer together. Eventually the turning points will coalesce.

2. Computation of the maximum radial mode number

As described in Chapter II, the maximum radial mode number is obtained by setting $\beta=k_2$, or according to (3-17), $\epsilon(\beta)=1$. Thus, (3-15) leads to

$$m_{max}=\frac{V}{\pi}\int_{\bar{r}_1}^{\bar{r}_2}\sqrt{\bar{r}^2-(\frac{\nu}{V})^2+\bar{r}^{\alpha+2}}\;\frac{d\bar{r}}{\bar{r}}, \qquad (3\text{-}20)$$

where the turning points which correspond to the maximum m will then satisfy

$$\bar{r}^{\alpha+2}-\bar{r}^2+(\frac{\nu}{V})^2=0. \qquad (3\text{-}21)$$

3. Computation of the maximum azimuthal mode number

The first step in obtaining the maximum azimuthal mode number ν_{max} is to find $\nu(r_p)$ as represented in Figure 4. There is a peak in the function $\nu(r)$ already defined by (2-15). The second step is to evaluate the expression for the limiting

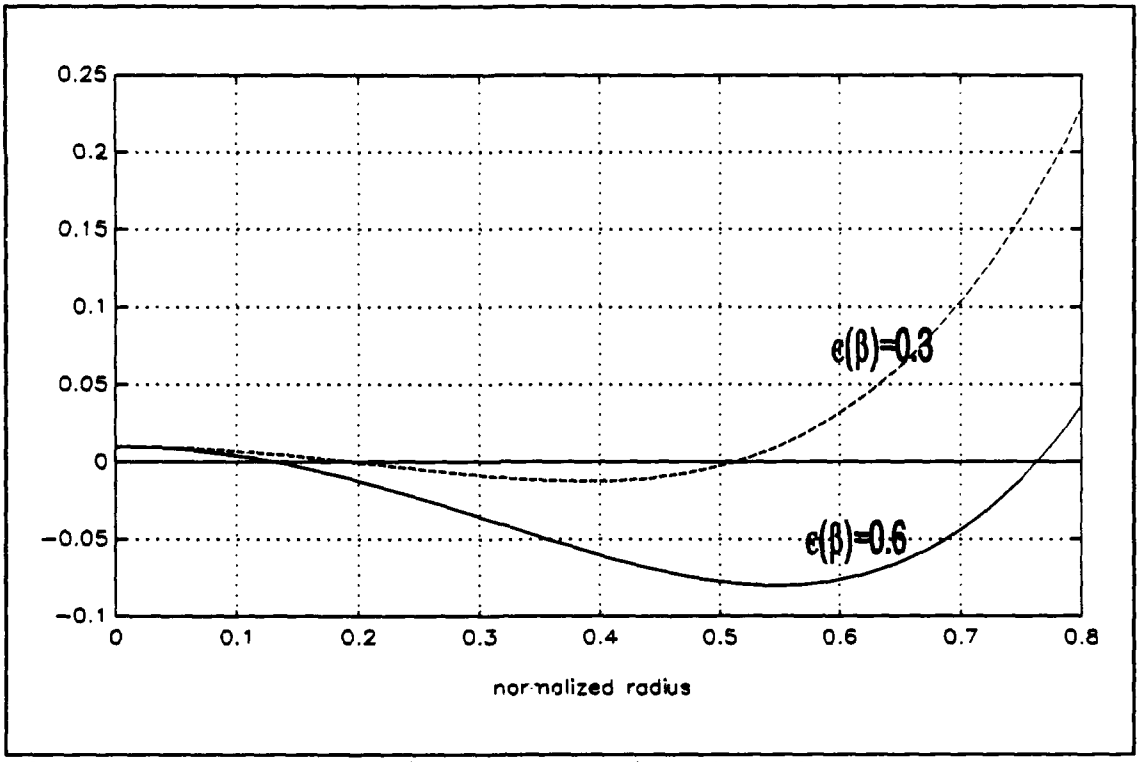

Figure 6: Left hand side of Equation (3-19).

condition $\beta=kn_2$.

Combining the power profile (3-13) with (2-15) leads to

$$v^2=r^2\left\{k^2n_1^2[1-2\Delta(\frac{r}{\alpha})^{\alpha}]-\beta^2\right\}. \qquad (3\text{-}22)$$

By evaluating

$$\frac{d}{dr}(v^2)=0, \qquad (3\text{-}23)$$

it can be shown that

$$\bar{r}_p^{\alpha}=\frac{n_1^2-\frac{\beta^2}{k^2}}{n_1^2\Delta(2+\alpha)} \qquad (arbitrary\ v), \qquad (3\text{-}24)$$

which for the limit condition $\beta=kn_2$, leads to

$$\bar{r}_p=\left(\frac{2}{2+\alpha}\right)^{\frac{1}{\alpha}} \qquad (\nu=\nu_{max}), \tag{3-25}$$

where $\bar{r}_p$ is the normalized radius extremum given by

$$\bar{r}_p=\frac{r_p}{a}. \tag{3-26}$$

Finally, from substitution of (3-25) into (3-24), we have

$$\nu_{max}=V\left(\frac{2}{2+\alpha}\right)^{\frac{1}{\alpha}}\sqrt{\frac{\alpha}{2+\alpha}}, \tag{3-27}$$

which shows that ν_{max} depends on the α profile and the V-parameter.

4. Computation of the evolution equations

Through combinations of (3-2), (3-3), (3-5) and (3-6) we have that

$$\frac{dz}{dr}=\frac{d\bar{z}}{d\bar{r}}=\frac{k_z}{k_r}=\frac{\beta}{k_r}=\frac{ctn\theta}{\cos\xi}, \tag{3-28}$$

where

$$\bar{z}=\frac{z}{a} \tag{3-29}$$

is the normalized z component of the ray.

It is easy to demonstrate from (2-11), (2-12) and (3-15) that

$$k_r = \frac{V}{r}\sqrt{\epsilon(\beta)\,\bar{r}^2 + f(r) - \left(\frac{\nu}{V}\right)^2 - \bar{r}^{\alpha+2}}\,, \tag{3-30}$$

and from (3-16) and (3-17) that

$$\beta = \frac{\sqrt{n_1^2 - NA^2\epsilon(\beta)}}{a\ NA}\,. \tag{3-31}$$

Substitution of (3-30) and (3-31) into (3-28) leads to

$$\frac{d\bar{z}}{d\bar{r}} = \frac{\sqrt{n_1^2 - NA^2\epsilon(\beta)}}{NA}\,\frac{\bar{r}}{\sqrt{\epsilon(\beta)\,\bar{r}^2 - \left(\frac{\nu}{V}\right)^2 - (\bar{r})^{2+\alpha}}}\,, \tag{3-32}$$

which is the evolution equation for the normalized z component of the ray.

Working similarly for the normalized ϕ component of the ray, combination of (3-1), (3-3), (3-6) and (3-7) gives

$$r\frac{d\phi}{dr} = \frac{k_\phi}{k_r} = \frac{-\frac{\nu}{r}}{\sqrt{k^2 n^2(r) - \beta^2 - \left(\frac{\nu}{r}\right)^2}} = \tan\xi\,, \tag{3-33}$$

and after substitution of (3-30) leads to

$$\frac{d\phi}{d\bar{r}} = -\frac{\nu}{V}\frac{1}{\bar{r}}\,\frac{1}{\sqrt{\epsilon(\beta)\,\bar{r}^2 - \left(\frac{\nu}{V}\right)^2 - \bar{r}^{\alpha+2}}}\,, \tag{3-34}$$

which is the evolution equation for the normalized ϕ component of the ray. Equations (3-32) and (3-34), which describe the ray trajectories, are shown to be in agreement with the Eikonal solution [Ref. 9] in Appendix B. Unlike the Eikonal

evolution equations, (3-32) and (3-34) are expressed in terms of the azimuthal mode number and the phase constant associated with the radial mode number (2-13).

The procedure describing the general approach applied in subsequent chapters is summarized in Appendix A.

IV. MERIDIONAL RAYS

In this chapter attention is given to meridional rays. It is well known that modal dispersion can be approximated fairly well through consideration of the meridional rays only [Ref. 1]. In the first section, the treatment for an arbitrary α parameter is presented. In the last section, some conclusions for the specific case of step index fibers are then presented.

A. GRADED INDEX MERIDIONAL RAYS WITH ARBITRARY α

Meridional rays are rays which pass through the z axis, and according to (2-8), have no rotational component, that is,

$$\nu = 0 \Leftrightarrow k_\phi = 0 . \tag{4-1}$$

For a power profile given by (3-13), it follows from (4-1) that (3-15) and (3-20) simplify for this case to

$$m = \frac{V}{\pi}\int_0^{\bar{r}_1} \sqrt{\epsilon(\beta)\,\bar{r}^2 - \bar{r}^{\alpha+2}}\;\frac{d\bar{r}}{\bar{r}} \tag{4-2}$$

and

$$m_{max} = \frac{V}{\pi}\int_0^{\bar{r}_1} \sqrt{\bar{r}^2 - \bar{r}^{\alpha+2}}\;\frac{d\bar{r}}{\bar{r}}, \tag{4-3}$$

respectively. It is noted that the lower limit of integration in (4-2) and (4-3) is zero since the associated integrands have a root at $\bar{r}=0$. This agrees with the physical interpretation consistent with Figure 7, which represents the

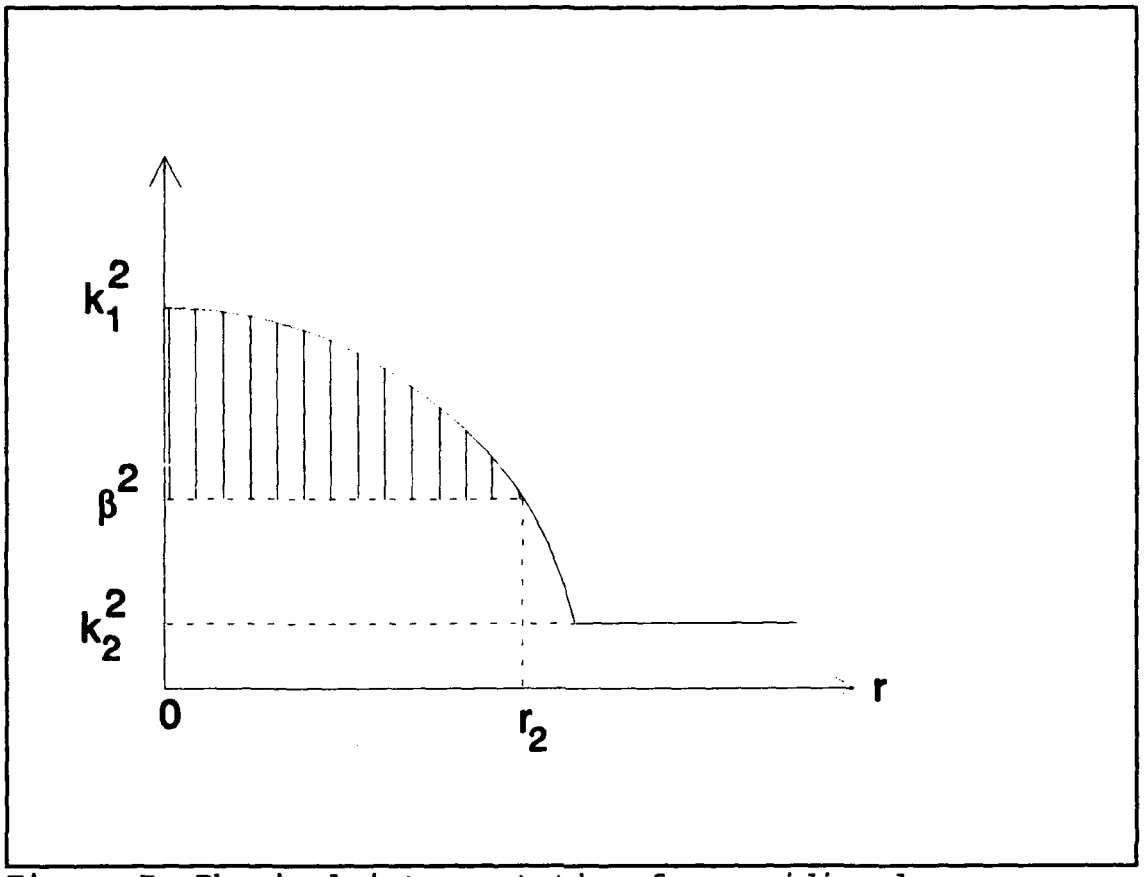

Figure 7: Physical interpretation for meridional rays.

special case $\nu=0$ of Figure 3. Equation (4-2) can be rewritten as

$$m=\frac{V\sqrt{\epsilon(\beta)}}{\pi}\int_0^{\bar{r}_2}\sqrt{1-\frac{\bar{r}^\alpha}{\epsilon(\beta)}}\,d\bar{r}, \tag{4-4}$$

and therefore, the second turning point will, from (4-4), satisfy

$$\bar{r}_2=(\epsilon(\beta))^{\frac{1}{\alpha}}. \tag{4-5}$$

After the variable substitution

$$u \equiv \frac{\bar{r}}{\bar{r}_2} = \frac{\bar{r}}{(\epsilon(\beta))^{\frac{1}{\alpha}}}, \tag{4-6}$$

we find

$$m = \frac{V \epsilon(\beta)^{\frac{2+\alpha}{2\alpha}}}{\pi} F(\alpha), \tag{4-7}$$

where

$$F(\alpha) \equiv \int_0^1 \sqrt{1-u^\alpha}\, du. \tag{4-8}$$

Although a general solution to (4-8) for all α does not appear possible, the integral $F(\alpha)$ is easily computed via numerical simulation (see Figure 8). The functions $F_1(\alpha)$ and $F_2(\alpha)$ defined in Table 1 are seen in Figure 8 to agree with $F(\alpha)$ for small and large α, respectively. The analytic properties of $F(\alpha)$ are discussed in detail in Appendix D. Table 1 summarizing this discussion is provided here.

α	$F(\alpha)$
1	2/3
2	$\pi/4$
0	0 (non-physical)
∞	1
$\alpha \gg 1$	$F_1(\alpha) = (2\alpha+1)/(2\alpha+2)$
$\alpha \ll 1$	$F_2(\alpha) = (\alpha\pi)^{1/2}/2$

Table 1: Values for $F(\alpha)$.

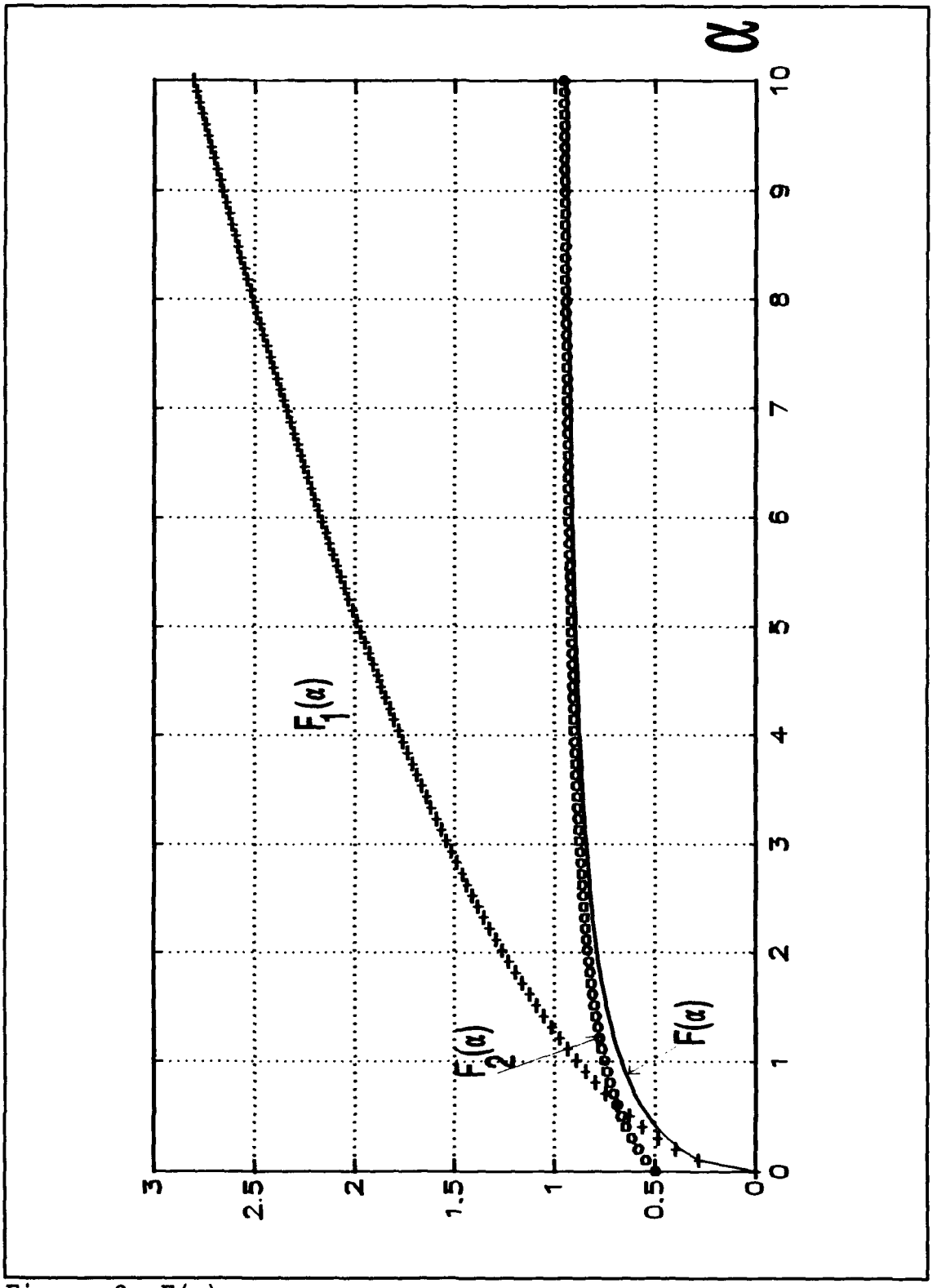

Figure 8: F(α) versus α.

In order to evaluate m_{max} from (4-3), $\epsilon(\beta)$ is again set to one (see Chapter III Section B), in (4-7), leading to

$$m_{max} = \frac{V}{\pi} F(\alpha) . \qquad (4\text{-}9)$$

A representative meridional graded index ray trajectory is shown in Figure 9.

Before deriving evolution equations for ray trajectories, we observe from (2-10) and (3-2) that

$$\beta = k\, n(r) \cos\theta_m(r) = k\, n_1 \cos\theta_{1m} \qquad (4\text{-}10)$$

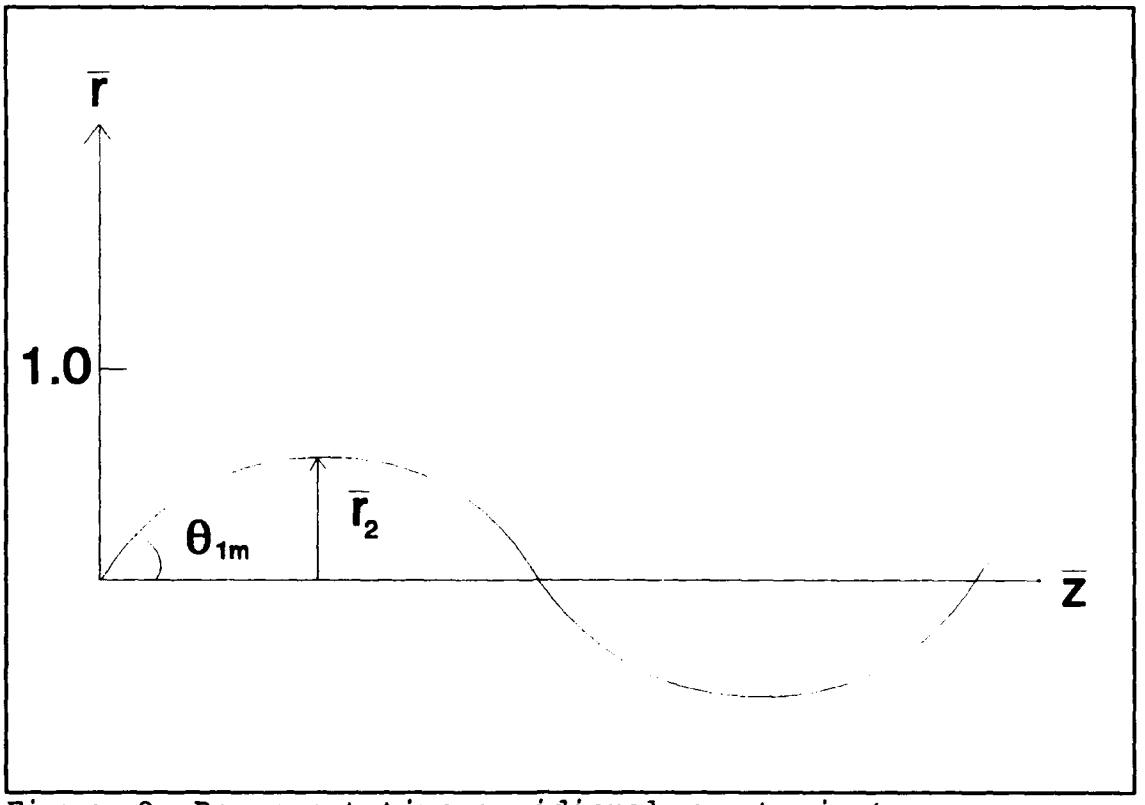

Figure 9: Representative meridional ray trajectory.

where the subscript "1" is to indicate evaluation at $n(r)=n_1$ (see (3-8)), and subscript m is to indicate a discrete angle associated with a specific radial mode. A geometrical interpretation which relates the angle θ_{1m} to m can be made. After substituting (4-10) into (3-17) we get

$$\epsilon(\beta)=\frac{n_1^2\sin^2\theta_{1m}}{NA^2}, \tag{4-11}$$

which when substituted into (4-7) provides a relationship between θ_{1m} and m as

$$\sin\theta_{1m}=\frac{NA}{n_1}\left(\frac{\pi m}{V}\frac{1}{F(\alpha)}\right)^{\frac{\alpha}{\alpha+2}}, \tag{4-12}$$

which is in agreement with Figure 2.

For calculation of $\bar{z}(\bar{r})$, we see that (3-32) simplifies under condition (4-1) to

$$\frac{d\bar{z}}{d\bar{r}}=\frac{\sqrt{n_1^2+NA^2\epsilon(\beta)}}{NA}\frac{\bar{r}}{\sqrt{\epsilon(\beta)\bar{r}^2-(\bar{r})^{(\alpha+2)}}}. \tag{4-13}$$

After combinations of (3-17), (4-10), and (4-11), $\bar{z}(\bar{r})$ takes on the integral form

$$\bar{z}(\bar{r})=\frac{n_1\cos\theta_{1m}}{n_1\sin\theta_{1m}}\int_0^{\bar{r}}\frac{d\bar{r}}{\sqrt{1-\left(\frac{\bar{r}}{\bar{r}_2}\right)^{\alpha}}}. \tag{4-14}$$

After use of (4-6), it is easily seen that

$$\bar{z}(\bar{r}) = \bar{r}_2 ctn\theta_{1m} \int_0^{\frac{\bar{r}}{\bar{r}_2}} \frac{du}{\sqrt{1-u^\alpha}}, \qquad (4\text{-}15)$$

where $\bar{r} \epsilon [0, \bar{r}_2]$. The parameter $\bar{r}_2$ is defined in terms of m through (4-5), (4-11), and (4-12) which leads to

$$\bar{r}_2 = \left(\frac{\pi m}{V} \frac{1}{F(\alpha)}\right)^{\frac{2}{\alpha+2}}. \qquad (4\text{-}16)$$

Again, as in the case of $F(\alpha)$, exact solutions for (4-14) and (4-15) can be found for α=1, α=2, and α=∞.

Because of condition (4-1), the azimuthal variation is zero. Therefore, there is no need to consider the ϕ variation described by (3-34). Appendix A summarizes the process of trajectory analysis for meridional rays also.

Figure 10 illustrates meridional rays plotted using (4-14) under conditions α=6, NA=0.5, V=100 and n_1=0.5. The curves are distinguished only by the radial mode numbers m=20 and m=2. As expected from Figure 2, m increases with k_r, and from (2-4), β decreases with m. Examination of Figure 6 confirms that the peak values of the trajectories increase with m. The values predicted from (4-16), $\bar{r}_2$=0.9114 for m=20 and $\bar{r}_2$=0.5125 for m=2, agree with the curves shown.

B. GRADED INDEX MERIDIONAL RAYS WITH α=2

Equations (4-9), (4-12), (4-15) and (4-16) can be evaluated for α=2. From Table 1, (4-9), (4-12), and (4-16) become

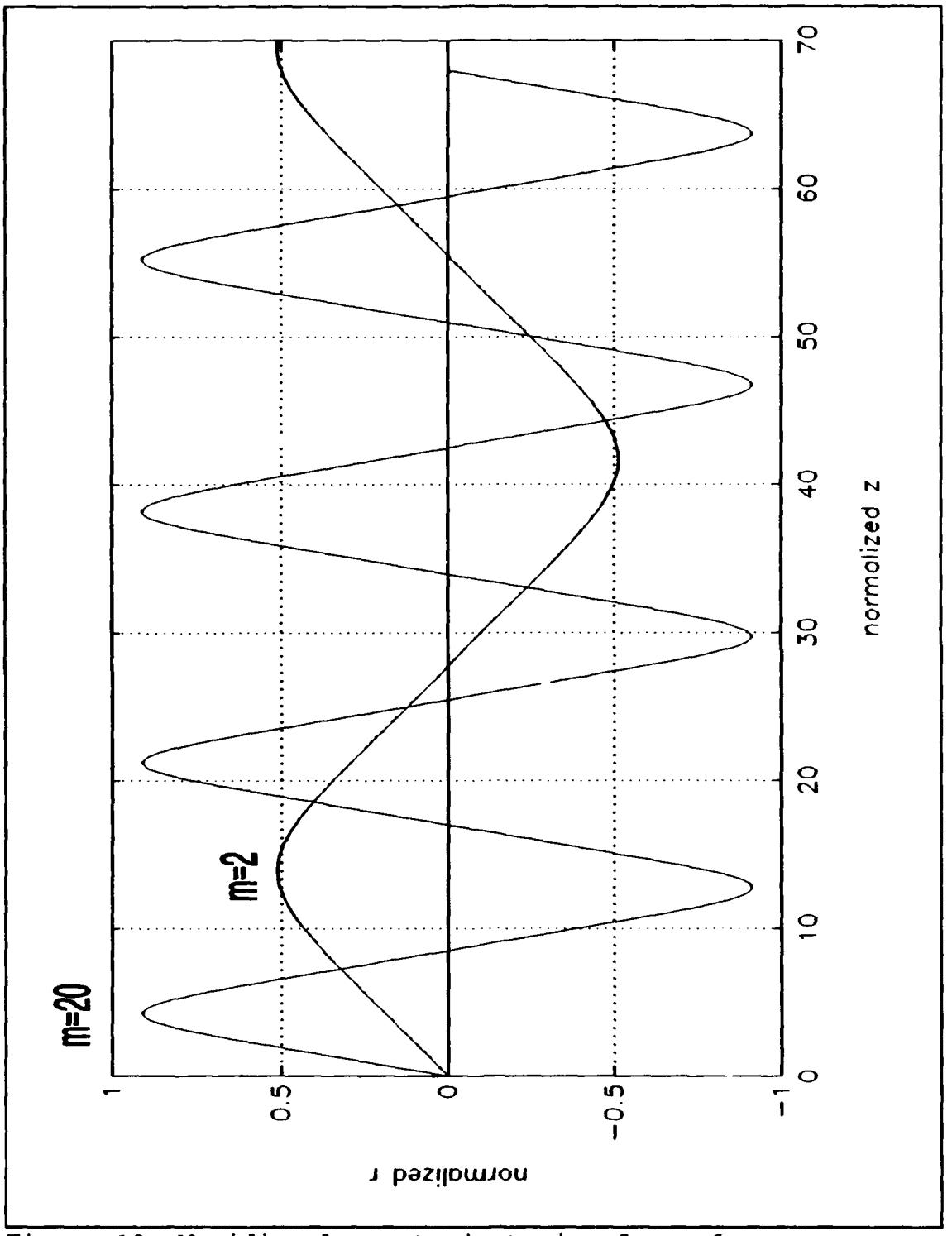

Figure 10: Meridional ray trajectories for α=6.

$$m_{max}=Int[\frac{V}{4}], \tag{4-17}$$

$$\sin\theta_{lm}=\frac{NA}{n_1}\sqrt{\frac{4m}{V}} \tag{4-18}$$

and

$$\bar{r}_2=\sqrt{\frac{4m}{V}}, \tag{4-19}$$

respectively. And lastly, through use of the integral [Ref. 18]

$$\int_0^1 \frac{du}{\sqrt{1-u^2}}=\arcsin u, \tag{4-20}$$

the trajectory equation (4-15) can be expressed as

$$\bar{r}=\bar{r}_2\sin(\frac{\bar{z}}{\bar{r}_2 ctn\theta_{lm}}). \tag{4-21}$$

Therefore, for α=2, the trajectory shape is exactly sinusoidal with a normalized $\bar{z}$ period

$$\Lambda_m=2\pi\bar{r}_2 ctn\theta_{lm}, \tag{4-22}$$

defined in terms of the specific initial condition of the angle of the ray as it crosses the normalized z axis. From (4-18) and (4-19), the dependence of the normalized period on V,NA and m is given by

$$\Lambda_m = 2\pi\sqrt{X-Y}\,, \tag{4-23}$$

where

$$Y = \frac{4m}{V}\,, \tag{4-24}$$

and

$$X = \left(\frac{n_1}{NA}\right)^2. \tag{4-25}$$

Figure 11 is a plot of Λ_m for typical values of X.

Figure 12 shows two meridional rays plotted using (4-22) under conditions α=2, NA=0.5, V=100 and n_1=1.5. The curves are only distinguished by the radial mode numbers m=20 and m=2. As expected from (4-19), the peak value of the trajectories are $\bar{r}_2$=0.894 for m=20 and $\bar{r}_2$=0.282 for m=2. Also, it can be seen from the X=9 curve of Figure 11, that the period for m=2 is approximately 19 and the period for m=20 is 18.

C. STEP INDEX MERIDIONAL RAYS

By definition, for step index meridional rays, in the limit as

$$\alpha \to \infty\,, \tag{4-26}$$

which when substituted into (3-27) gives

$$\nu_{max} = Int[V]\,. \tag{4-27}$$

The peak turning point can be found by substituting (4-1) and (4-26) into (3-25) yielding

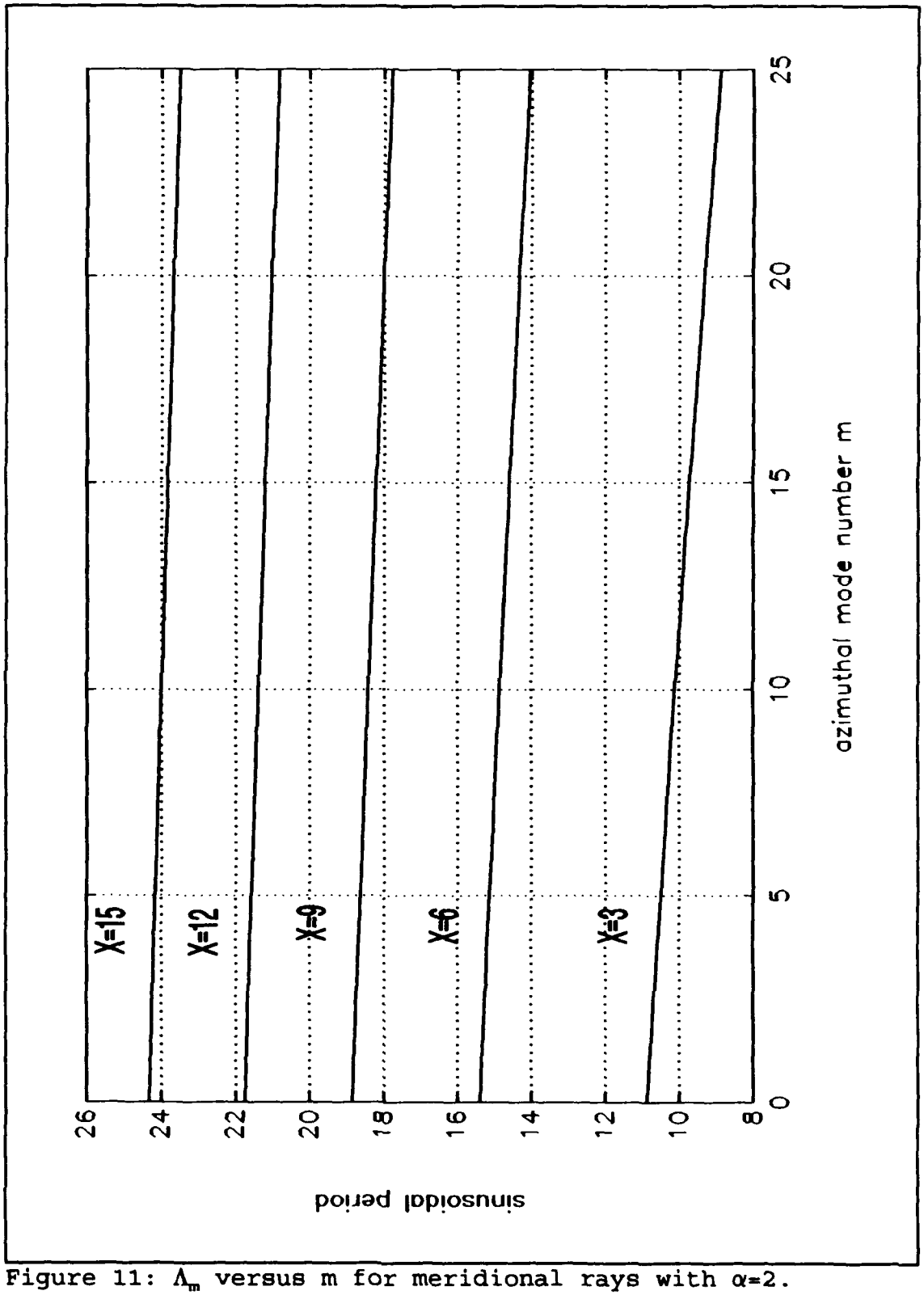

Figure 11: Λ_m versus m for meridional rays with α=2.

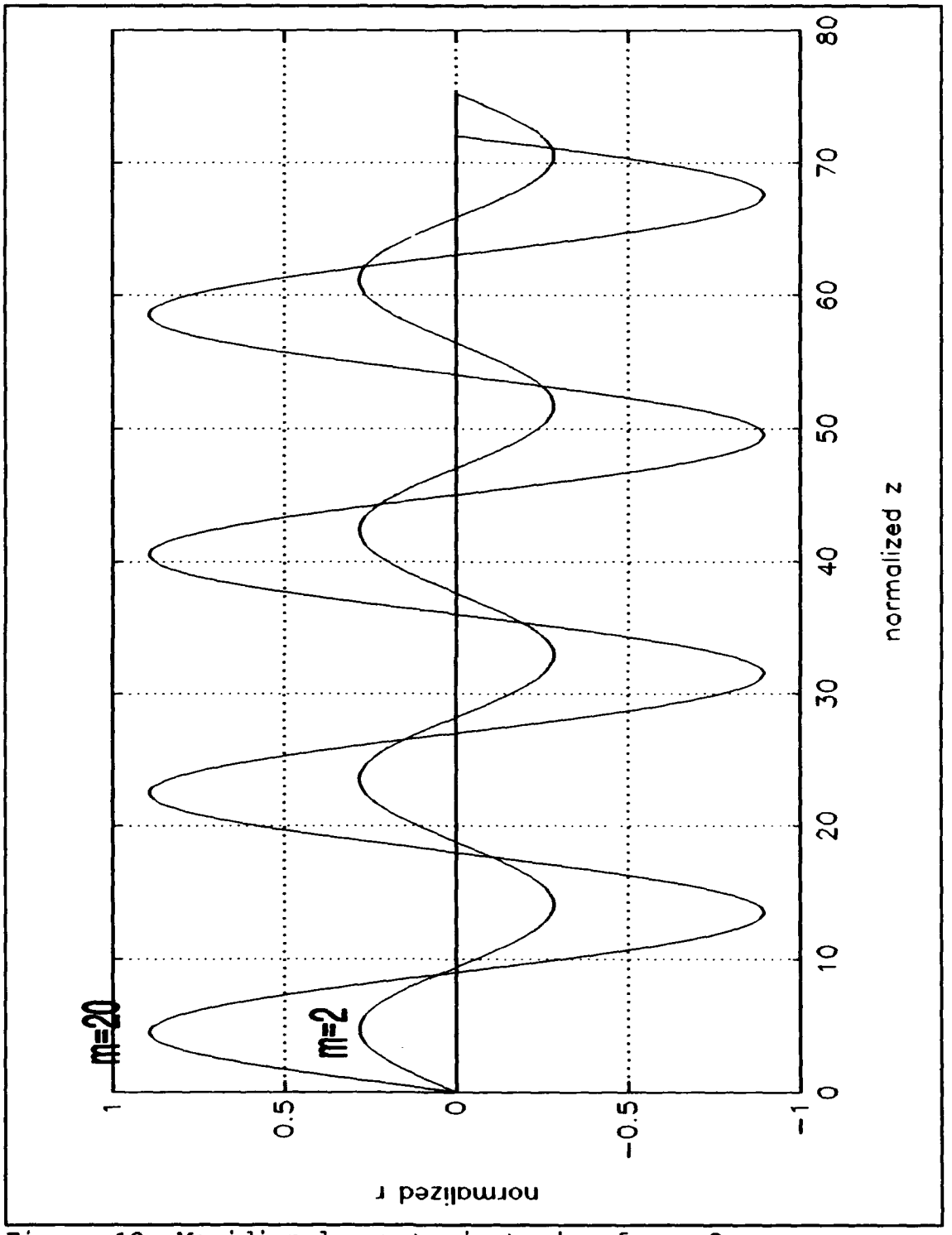

Figure 12: Meridional ray trajectories for α=2.

$$\bar{r}_p=\bar{r}_2=1. \tag{4-28}$$

In order to find the maximum radial mode number (4-1), (4-26) and (4-28) are substituted into (3-20) which gives

$$m_{max}=Int[\frac{V}{\pi}]. \tag{4-29}$$

The evolution equation for the z component can be derived by substituting (4-26) into (3-28) yielding

$$\frac{d\bar{z}}{d\bar{r}}=ctn\theta. \tag{4-30}$$

The still unknown angle θ of (4-30) can be found from (2-12), which for this case takes the form

$$m=\frac{1}{\pi}\int_0^a kn_1\sin\theta\, dr. \tag{4-31}$$

By integrating (4-31) and eliminating a and k through combinations of (3-12) and (3-16), we have

$$\theta=\sin^{-1}(\frac{mNA\pi}{Vn_1}). \tag{4-32}$$

Finally, by integration of (4-30), we get

$$\bar{z}(\bar{r})=\bar{r}ctn\theta, \tag{4-33}$$

where according to (4-28), $\bar{r}\epsilon[0,1]$. Equations (4-32) and (4-33) are the basis for the simulations described in the next paragraph.

Figure 13 illustrates step index meridional rays plotted using (4-33) under conditions NA=0.5, V=100 and n_1=1.5. The

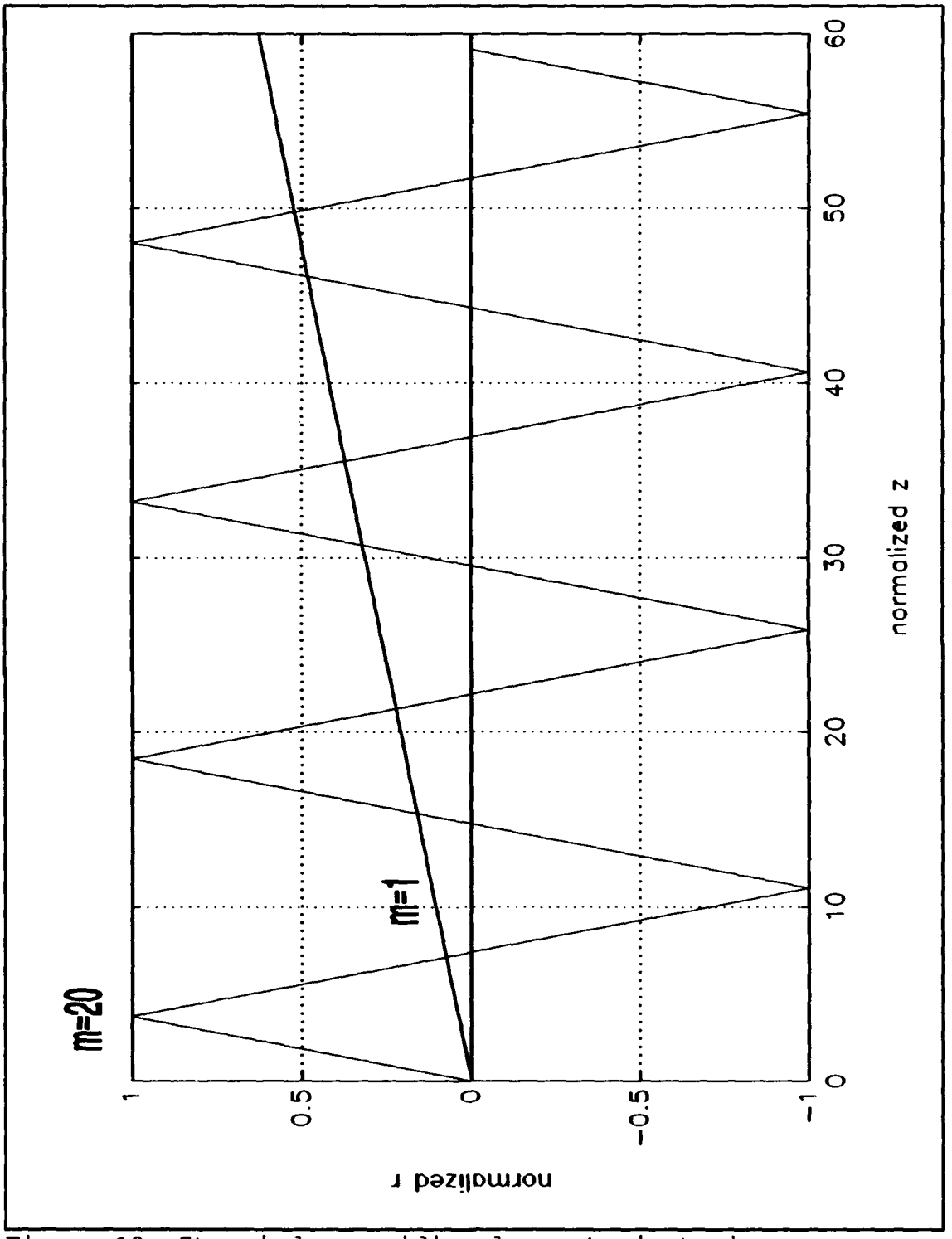

Figure 13: Step index meridional ray trajectories.

curves are only distinguished by the radial mode values m=1 and m=20. Although it is not apparent from Figure 13, as expected from (4-28), in both cases, $\bar{r}_p$=1.

D. FINAL REMARKS

In this chapter, the general equations of Chapter III are applied under conditions valid for meridional rays. An analytic form for the ray trajectories was established. The existence of a direct connection between the radial mode number m and the orientation angle θ has been demonstrated. This is a first sign that a link between Eikonal ray trajectories and mode numbers is possible. It is noted that although a three-dimensional perspective of meridional ray trajectories could have been demonstrated, the fact that the rotational component is zero (see (4-1)) made it unnecessary. In the chapters that follow, the analysis is applied to skew rays.

V. SKEW RAYS IN A STEP INDEX OPTICAL FIBER

A. INTRODUCTORY REMARKS

This Chapter presents a brief discussion for the analysis of skew rays in a step index fiber. It follows from (3-13) that the general results from Chapter III can be applied after taking the limit $\alpha \to \infty$. A more detailed description of this subject can be found in Appendix E. This appendix is a reproduction of a published work [Ref. 19] based on results obtained in the early stage of the thesis. One purpose of this chapter is to provide a clear link between the general formulation of Chapter III and the analytical approach for step index optical fibers described in Appendix E. Some additional results will also be presented. In this chapter the notation on the turning points will be modified to be in agreement with Appendix E. Specifically, the more suggestive labels of r_{min} and r_{max} will be used for r_1 and r_2, respectively.

B. OVERALL ANALYSIS

In this section the solutions in the step index case (in the limit as $\alpha \to \infty$) are obtained. It follows from Figure 14 that $\bar{r}_{max}=1$. This can be confirmed from (3-25)

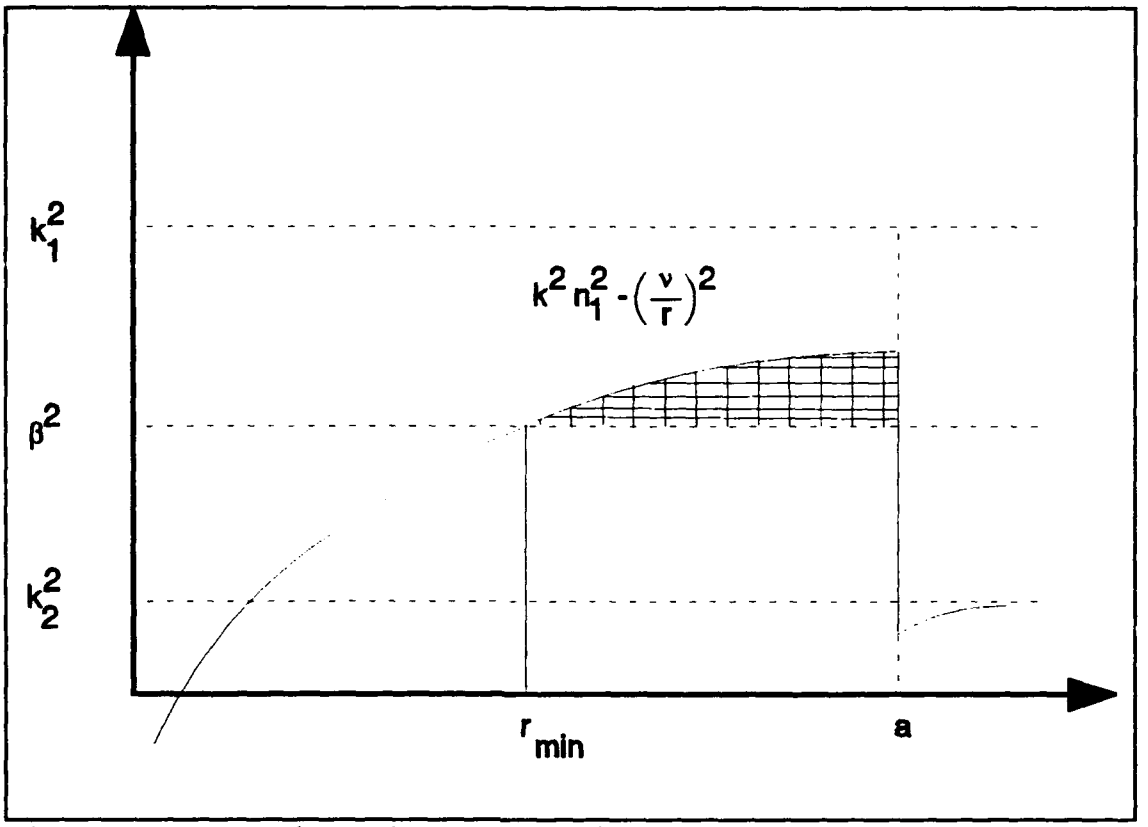

Figure 14: Physical interpretation for step index skew rays.

$$\bar{r}_{max} = \lim_{\alpha \to \infty} \left(\frac{2}{2+\alpha}\right)^{\frac{1}{\alpha}} \to 1. \tag{5-1}$$

It then follows from (3-15), after taking f(r)=0, that

$$m = \frac{V}{\pi} \int_{\bar{r}_{min}}^{1} \sqrt{\epsilon(\beta)\bar{r}^2 - \left(\frac{\nu}{V}\right)^2}\, d\bar{r}, \tag{5-2}$$

where the lower limit can be obtained from (3-19)

$$\bar{r}_{min} = \frac{\nu}{V\sqrt{\epsilon(\beta)}}. \tag{5-3}$$

After substitution of (5-3) into (5-2), we find that

$$m=\frac{\nu}{\pi}\int_{\bar{r}_{min}}^{1}\sqrt{\left(\frac{\bar{r}}{\bar{r}_{min}}\right)^2-1}\,\frac{d\bar{r}}{\bar{r}}, \tag{5-4}$$

which can be directly integrated using [Ref. 18]

$$\int\frac{\sqrt{u^2-a^2}}{u}du=\sqrt{u^2-a^2}-a\sec^{-1}\left(\frac{u}{a}\right), \tag{5-5}$$

which leads to

$$m=\frac{\nu}{\pi}\left[\sqrt{\left(\frac{1}{\bar{r}_{min}}\right)^2-1}-\sec^{-1}\left(\frac{1}{\bar{r}_{min}}\right)\right], \tag{5-6}$$

which apparently is not applicable for meridional rays ($\nu=0$) since r_{min} given by (5-3) for meridional rays is zero. This case has been covered in Chapter IV, Section C.

As in Chapter III, Section B, the computation of m_{max} requires setting $\epsilon(\beta)=1.0$. It follows from (5-2) that for $m=m_{max}$

$$\bar{r}_{min}=\left(\frac{\nu}{V}\right), \tag{5-7}$$

and the corresponding value of m_{max} is

$$m_{max}(\nu)=\frac{1}{\pi}\left[\sqrt{V^2-\nu^2}-\nu\sec^{-1}\left(\frac{V}{\nu}\right)\right], \tag{5-8}$$

obtained after substituting (5-7) into (5-6).

From (3-27) the maximum azimuthal mode number is obtained

$$\nu_{max}=V, \tag{5-9}$$

in the limit as $\alpha\to\infty$.

This section is provided as a link between the general formulation of Chapter III and the more detailed step index analysis contained in Appendix E. It is noted that (5-3), (5-7) and (5-8) are easily shown to be in agreement with (E-20), (E-21) and (E-23), respectively.

C. ADDITIONAL RESULTS

The results and discussion appearing in Appendix E were presented at an IEEE conference [Ref. 19]. Due to the limitation of space, only a set of representative trajectory curves were presented at the conference. The parameters for other trajectory examples are summarized in Table 7 in Appendix E. In order to illustrate the application of the program under limiting conditions, two additional examples are presented.

1. Example A. $\nu=1 \ll \nu_{max}=150$

As seen in Figures 15 and 16, the rays are nearly meridional. The value for $\bar{r}_{min}=0.0104$, which for $m=30$ and $\nu=1$, can be checked by use of (5-6). It is noted that the ϕ dependence on $\bar{r}$ is given by

$$\phi=\sec^{-1}\left(\frac{\bar{r}}{\bar{r}_{min}}\right). \qquad (5\text{-}10)$$

The trajectory lines are absolutely straight as expected in a step index fiber. In Figure 15, a full three-dimensional view of the trajectory is provided. It is noted that the

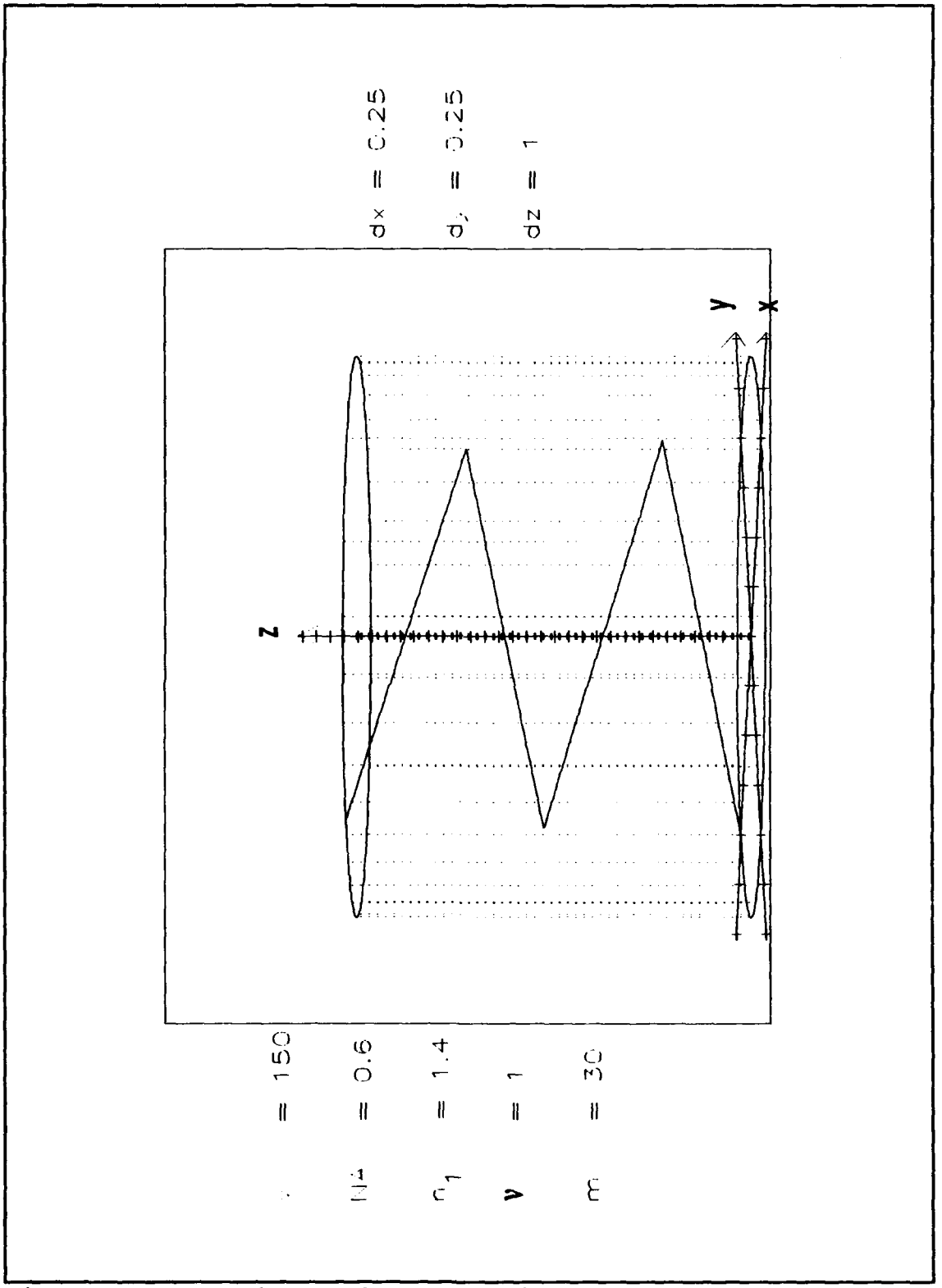

Figure 15: Step index skew rays with $\nu \ll \nu_{max}$.

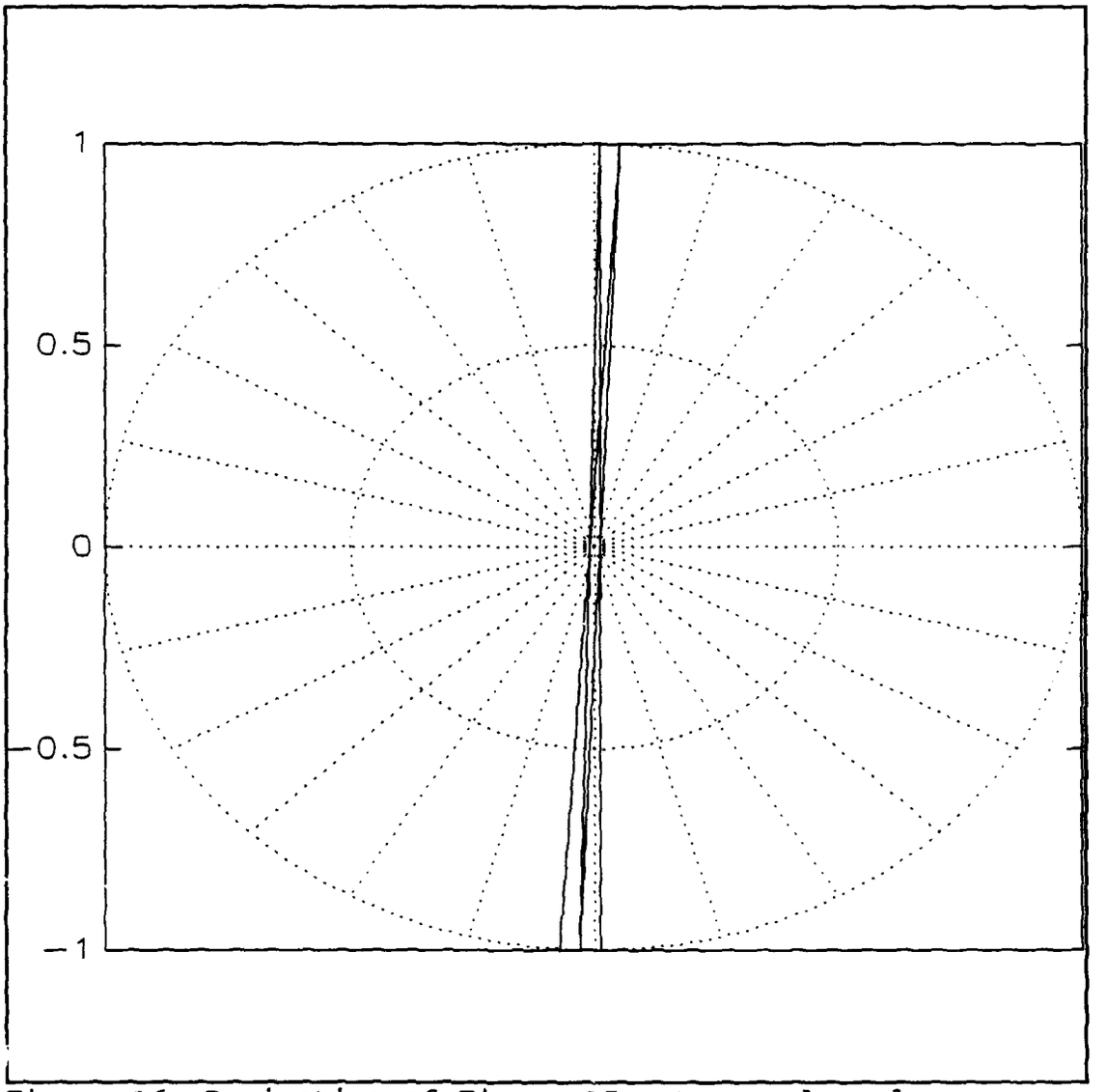

Figure 16: Projection of Figure 15 onto a polar plane.

trajectories continue out to $\bar{r}=1$, which can be seen from Figure 16.

2. Example B. $\nu=191\approx\nu_{max}=200$

Here ν was chosen to yield a value $\bar{r}_{min}$ that was much closer to one, i.e., a high rotational component. Again for m=1 and $\nu=191$, $\bar{r}_{min}=0.9358$ can be checked with (5-6) and Figure 17. The corresponding three-dimensional plot is Figure 18.

D. FINAL REMARKS

In this chapter ray trajectories were established from the general analysis of Chapter III with the only assumption that $\alpha\to\infty$. From Appendix E, we can see that the model relating the mode numbers m and ν with the orientation angles θ and ξ is very simple. Also, the three-dimensional perspective of ray trajectories shows that the model provides a good physical insight for a deeper understanding of optical fibers.

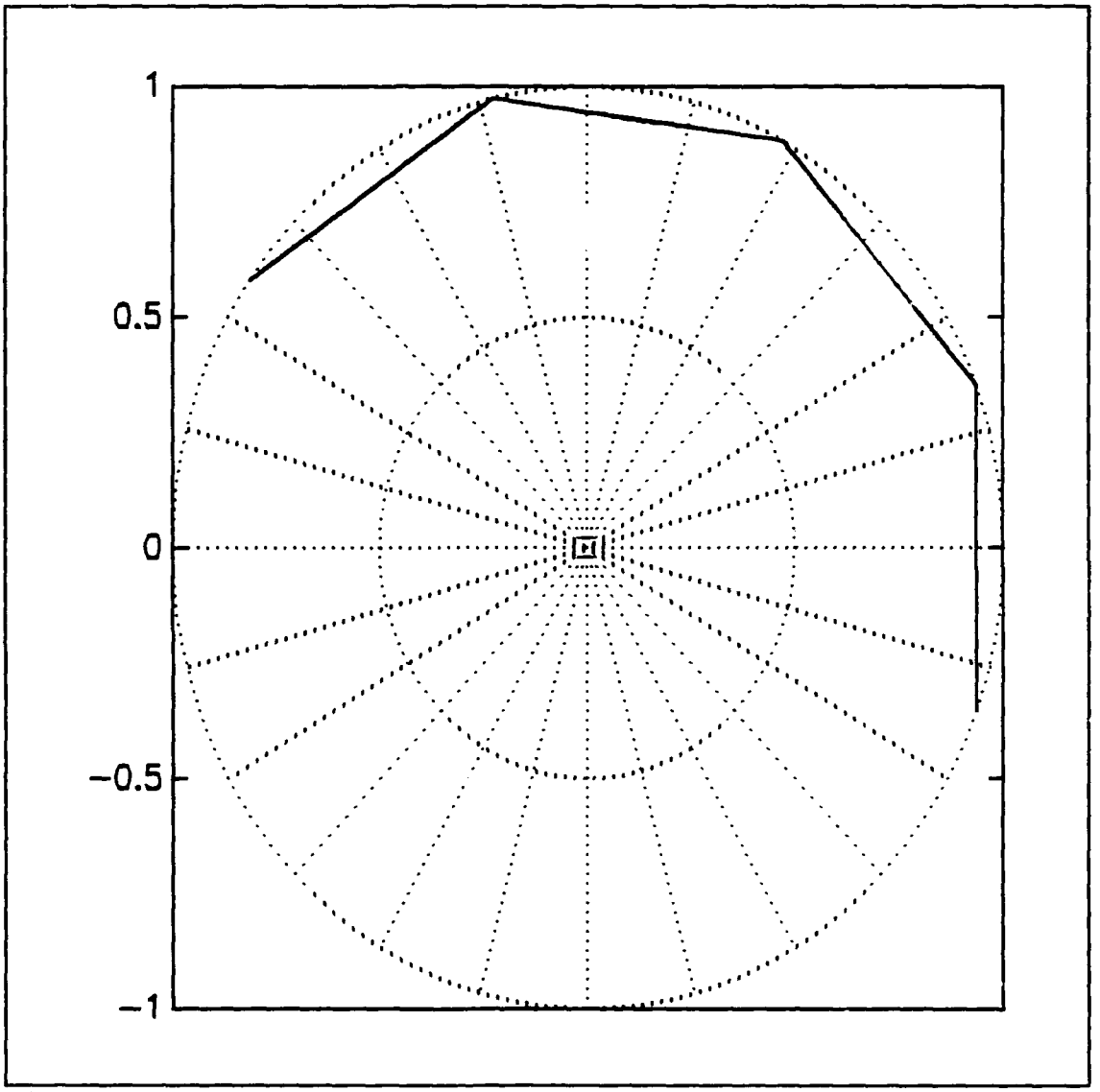

Figure 17: Polar projection for step index skew rays with $\nu \approx \nu_{max}$.

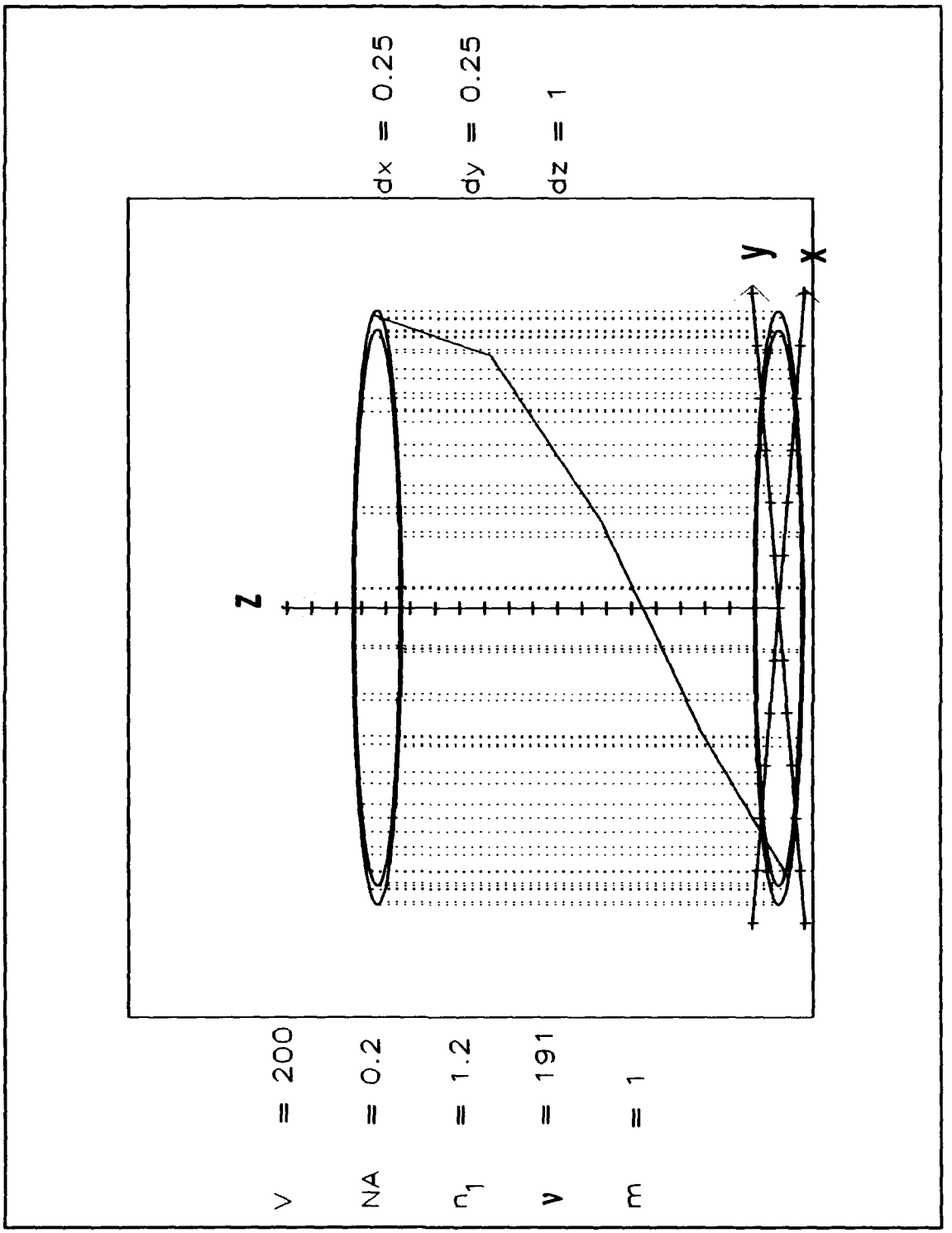

Figure 18: Three-dimensional representation of Figure 17.

VI. NUMERICAL SOLUTION FOR SKEW RAYS WITH ARBITRARY α

A. INTRODUCTORY REMARKS

The treatment for skew rays with arbitrary α requires the full generality of the analysis presented in Chapter III. Meridional rays, which are covered in Chapter IV, will not be treated here.

B. ANALYSIS

For the power profile given by (3-13), maximum azimuthal and radial mode numbers can be predicted from (3-27) and (3-20), respectively. Integral limits for (3-20) will satisfy (3-21).

In order to characterize the trajectories given by (3-32) and (3-34) associated with the ν and m modes, the normalized phase constant given by (3-17) and the turning points need to be accurately determined. In the most general case the problem does not have an analytic solution. In fact, the condition on the turning points $\bar{r}_1$ and $\bar{r}_2$, the normalized phase constant $\epsilon(\beta)$, and the radial mode number given by (3-15) need to be satisfied in a self consistent manner. The conceptual flowchart for this process is provided in Figure 19.

Finally, evolution equations can be predicted from the integral form of (3-32) and (3-34), which become

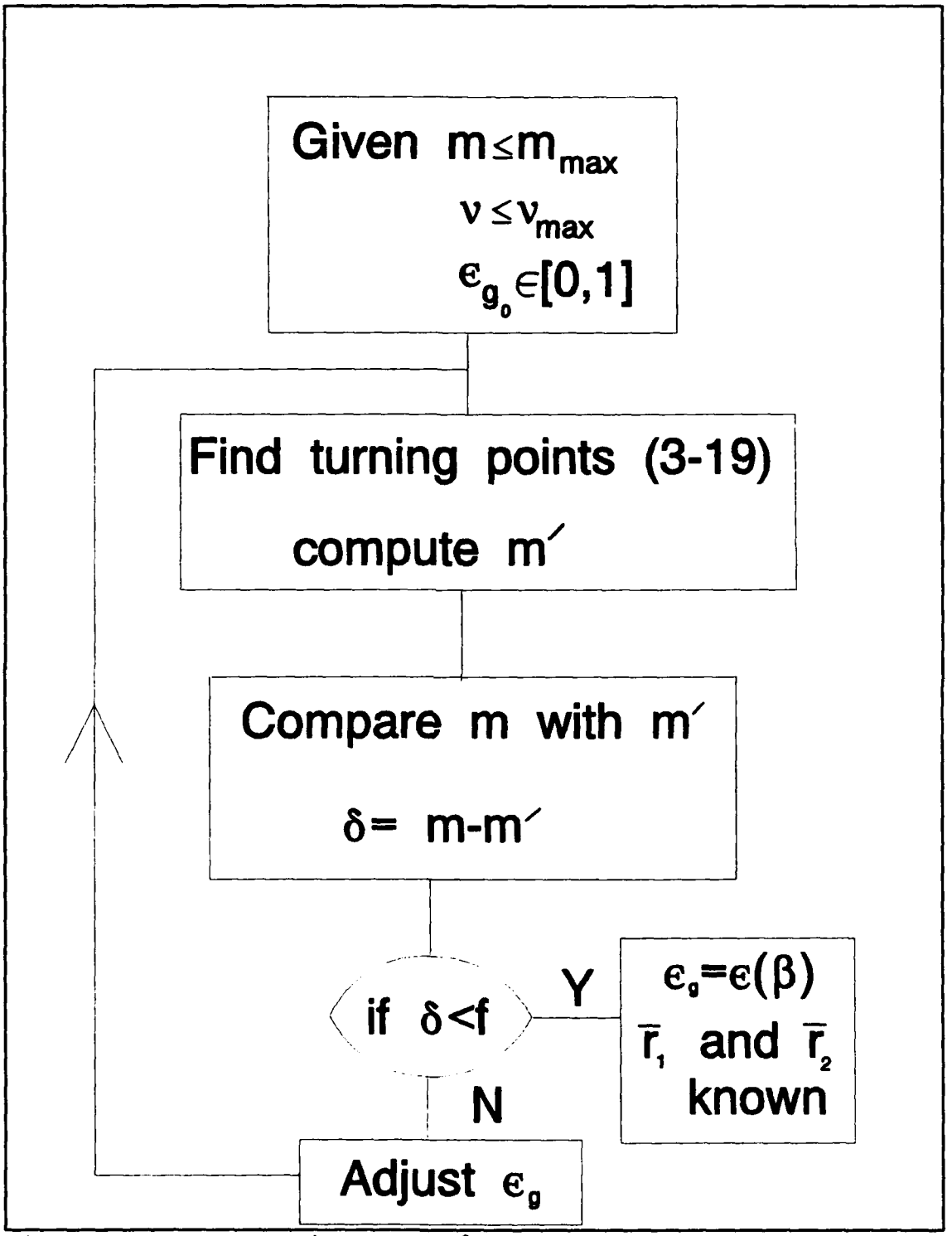

Figure 19: Calculation of $\epsilon(\beta)$ and turning points for skew rays with arbitrary α.

$$\bar{z}(\bar{r}) = \frac{\sqrt{n_1^2 - NA^2 \epsilon(\beta)}}{NA} \int_{\bar{r}_1}^{\bar{r}} \frac{\bar{r} d\bar{r}}{\sqrt{\epsilon(\beta)\bar{r}^2 - (\frac{\nu}{\bar{V}})^2 - (\bar{r})^{2+\alpha}}} \qquad (6\text{-}1)$$

and

$$\phi(\bar{r}) = -\frac{\nu}{\bar{V}} \int_{\bar{r}_1}^{\bar{r}} \frac{1}{\sqrt{\epsilon(\beta)\bar{r}^2 - (\frac{\nu}{\bar{V}})^2 - \bar{r}^{\alpha+2}}} \frac{d\bar{r}}{\bar{r}} \qquad (6\text{-}2)$$

respectively, where $\bar{r} \epsilon [\bar{r}_1, \bar{r}_2]$.

C. EXAMPLES

1. Ray trajectories

Figure 20 shows a three-dimensional plot of a numerically calculated skew ray trajectory from (6-1) and (6-2) using α=6. The dense vertical lines are drawn at $\bar{r}=\bar{r}_1$, and the low density lines are drawn at $\bar{r}=\bar{r}_2$. From Figure 20, $\Delta\bar{z}$ is defined as the axial distance between ray turning points $\bar{r}_1$ and $\bar{r}_2$. Because of the three-dimensional perspective, the normalized increment in $\Delta\bar{z}$ only appears to change size. Figure 21 shows the corresponding axial view. From Figure 21, $\Delta\phi$ is defined as

$$\Delta\phi = 2\arctan(\frac{\bar{r}_1}{\bar{r}_2}) . \qquad (6\text{-}3)$$

Figure 22 shows a ray trajectory with conditions given on the Figure with $\nu \approx \nu_{max}$. As can be seen from Figure 23, which is

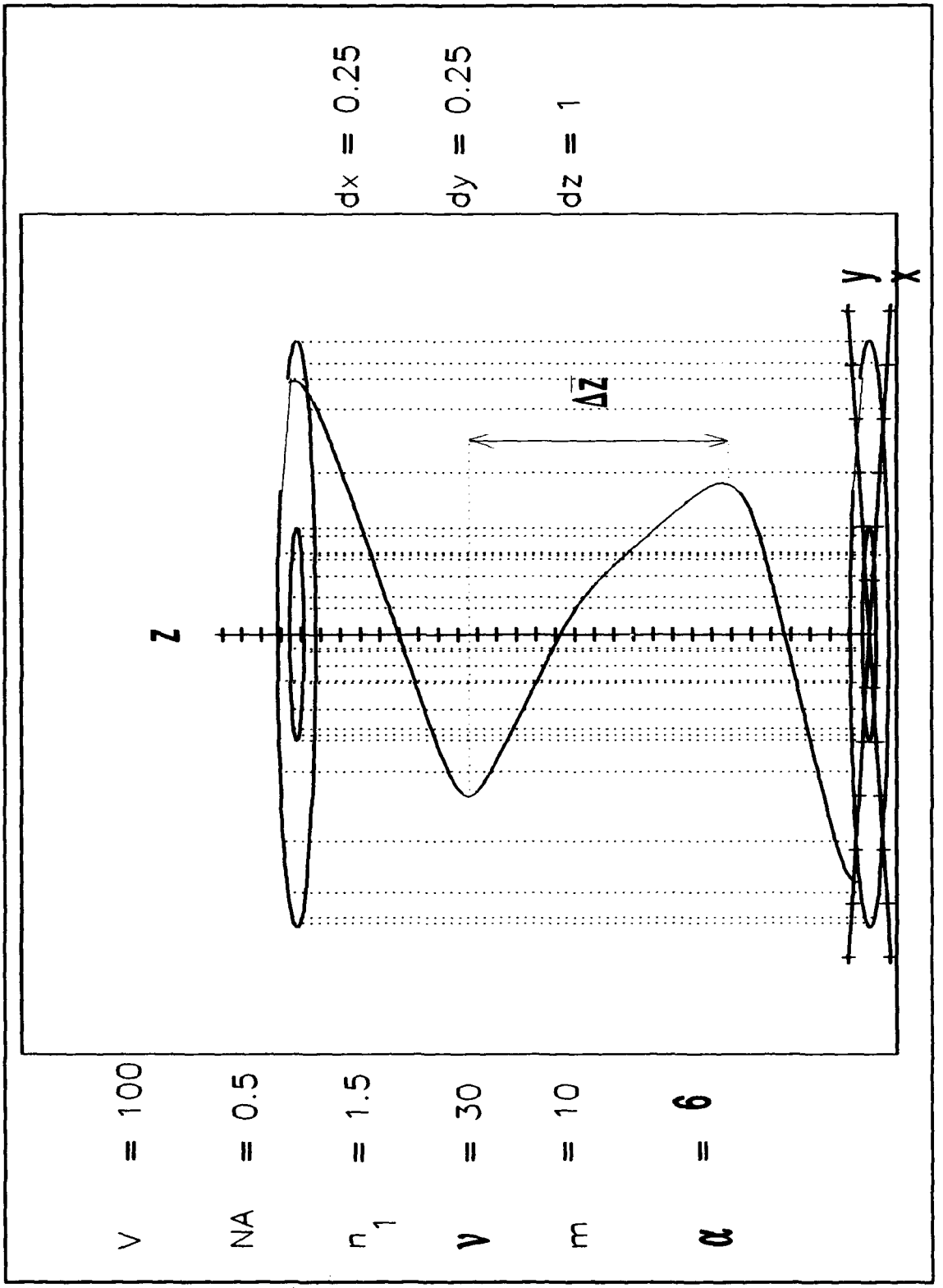

Figure 20: Ray trajectory for conditions as stated.

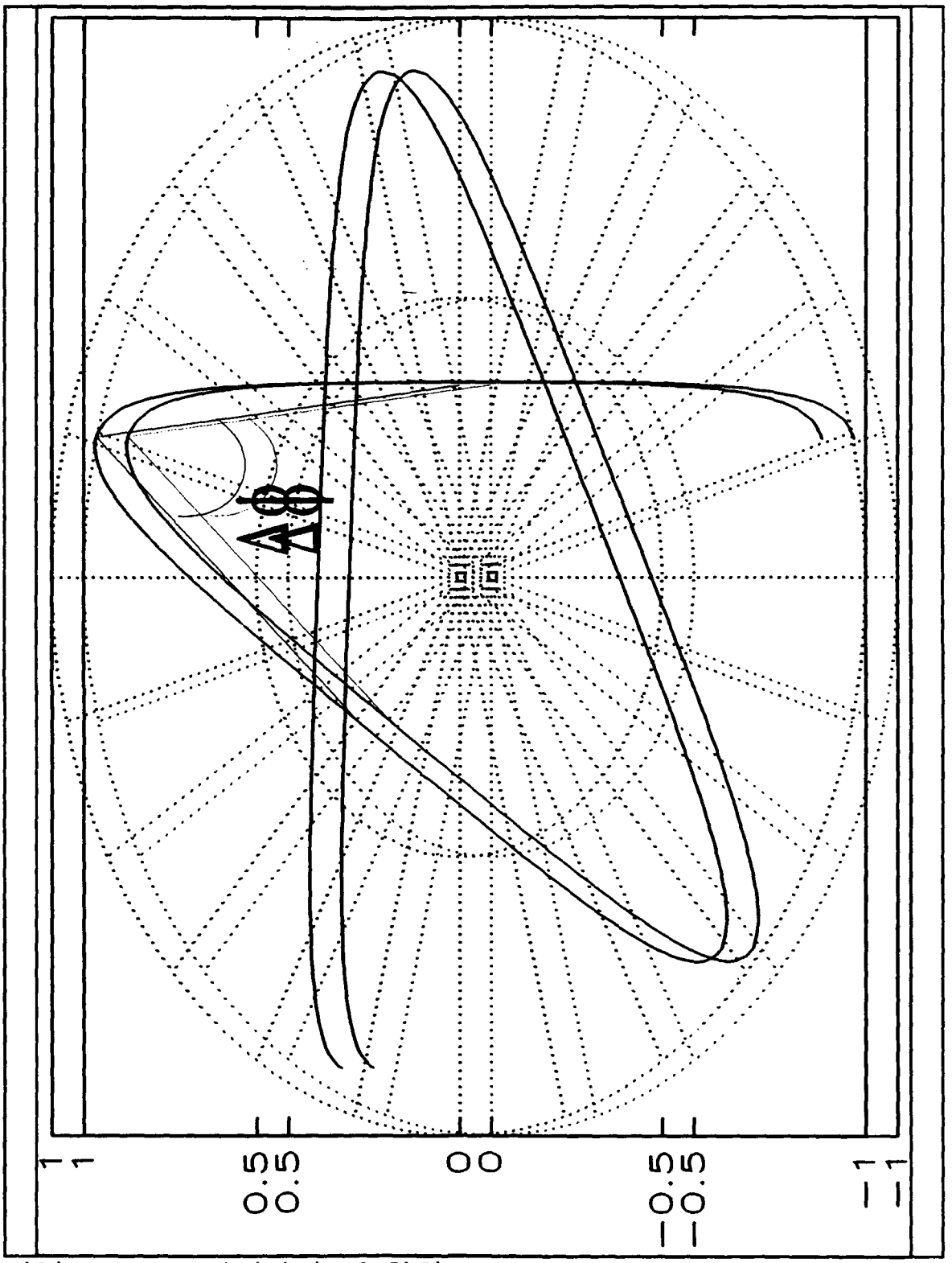

Figure 21 Projection of figure 20 onto a polar plane.

Best Available Copy

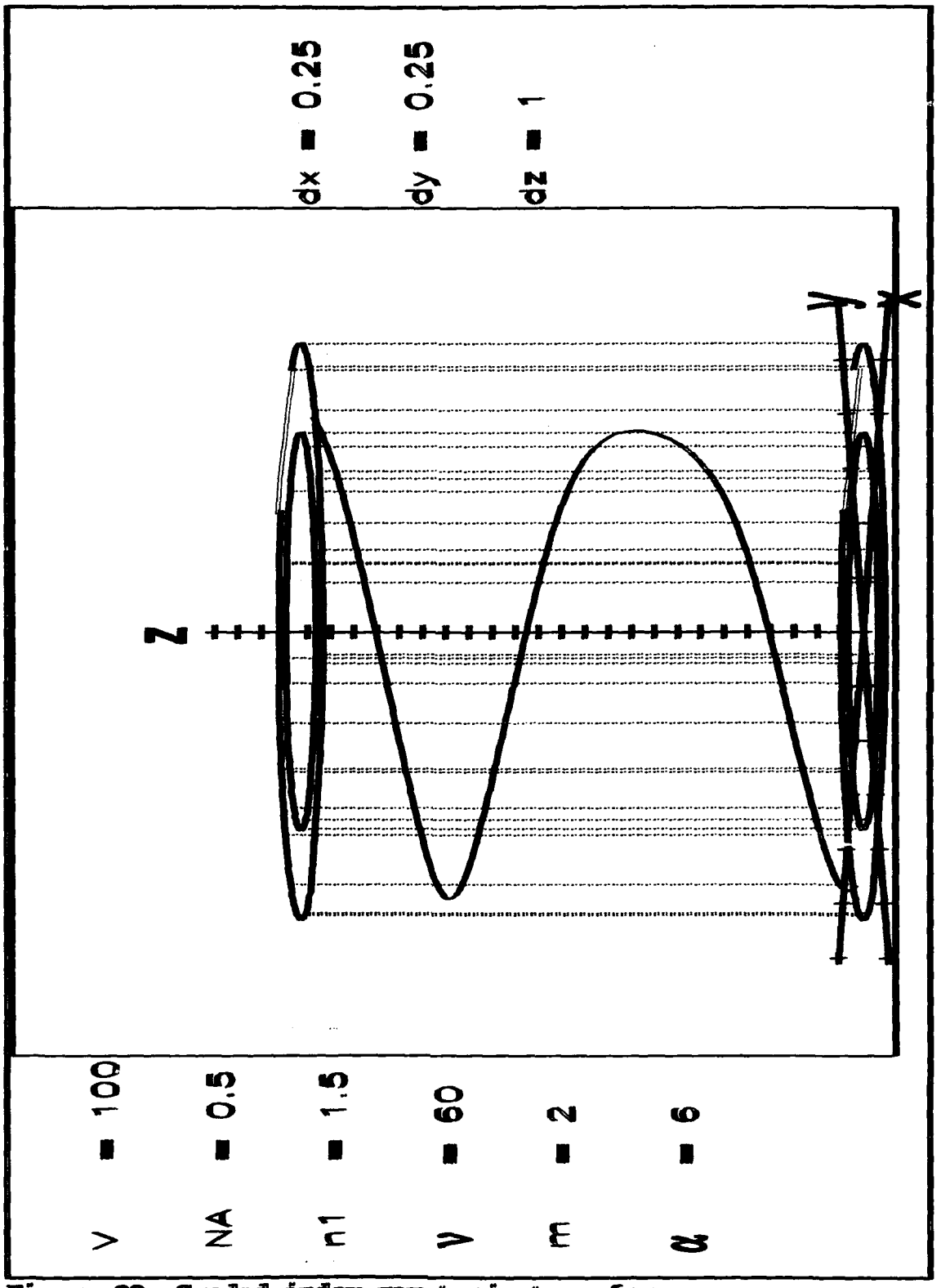

Figure 22: Graded index ray trajectory for ►►▬.

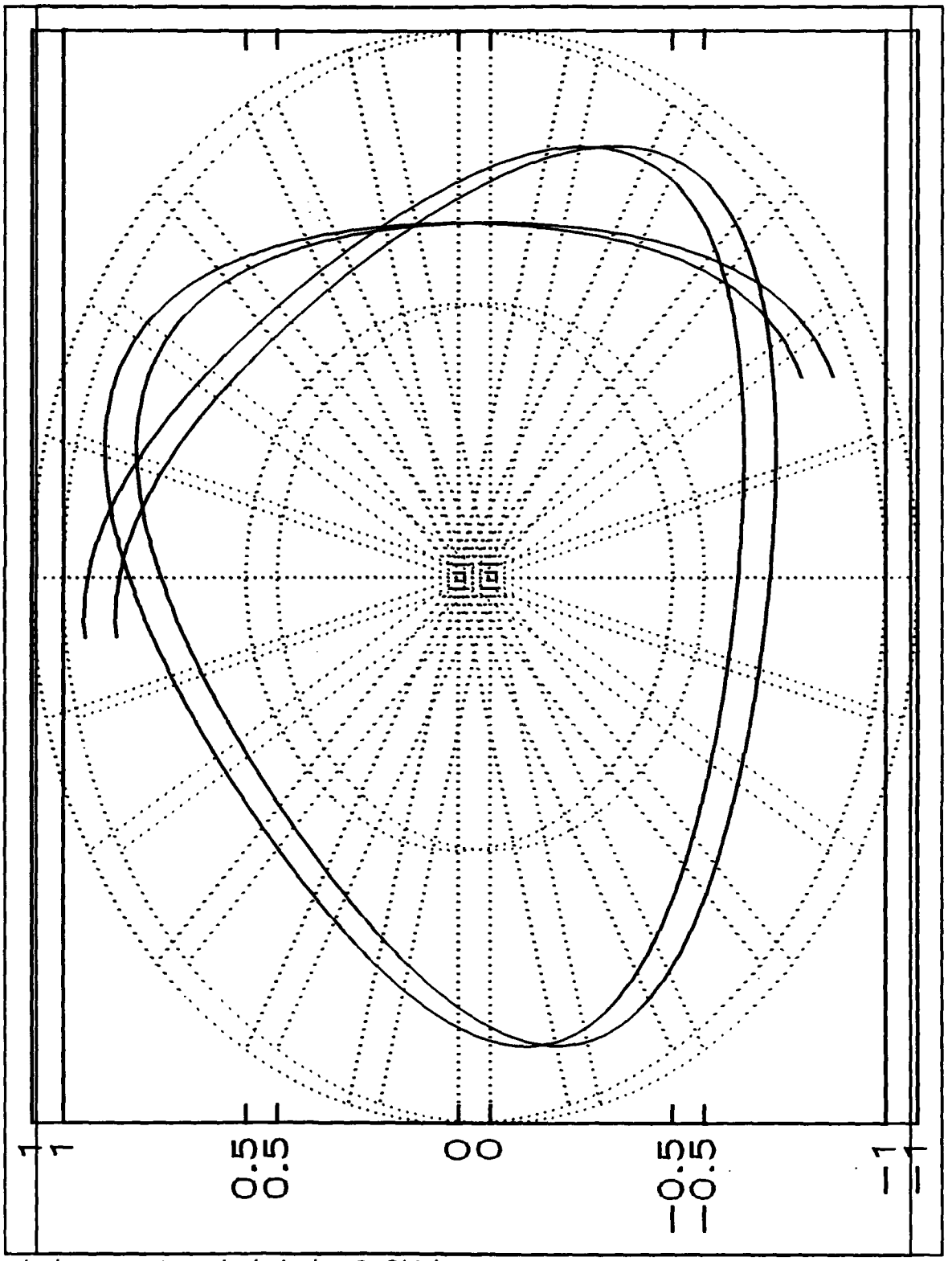

Figure 23 Projection of Figure 22 onto a polar plane.

Best Available Copy

the axial view of Figure 22, for this case, $\bar{r}_1$ is close to $\bar{r}_2$ as expected from Figure 3 for ν close to ν_{max}.

For the ray trajectories shown in Figure 24 and Figure 25, a very high value of α was chosen. As can be seen, the trajectories are indistinguishable from straight lines, as expected for rays in a step index fiber (as discussed in Chapter V for step index case in the limit as $\alpha \to \infty$).

The equations (6-1) and (6-2) were also numerically integrated for the case α=2. The three-dimensional perspective and axial views are shown on Figures 26 and 27, respectively. It is noted that in Figure 27, it is clear that the azimuthal orbit is closed. These results will be reexamined and explained in the next chapter.

2. Variation of fiber parameters

Table 2, Table 3 and Table 4 were derived from repeated applications of the optical conditions V=100, NA=0.5, n_1=1.5 and α as stated on the tables. The corresponding three-dimensional representations are seen in Figures 26, 20 and 22, respectively. The trends relating $\Delta\phi$ and $\Delta\bar{z}$ are readily explained. Because all of these tables have the same kind of variation of parameters, discussion will be concentrated on Table 2. In the lower half of the table, m is held constant at the value 10 while ν varies between 4 and 16. As ν increases, the angle $\Delta\phi$ increases with the rotational component, k_ϕ, as expected. It is clear from (2-13) (or in normalized form from

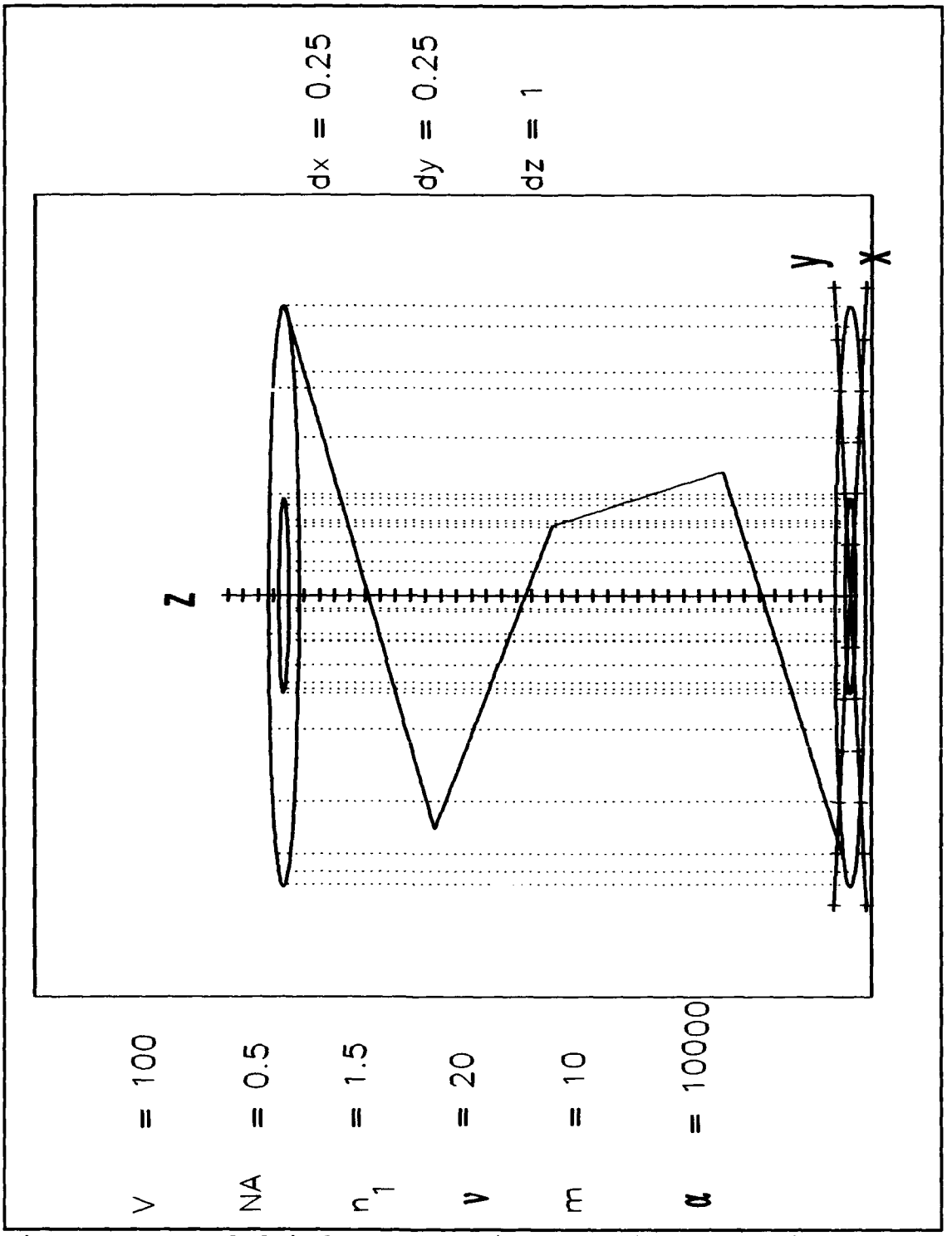

Figure 24: Graded index ray trajectory with very high α.

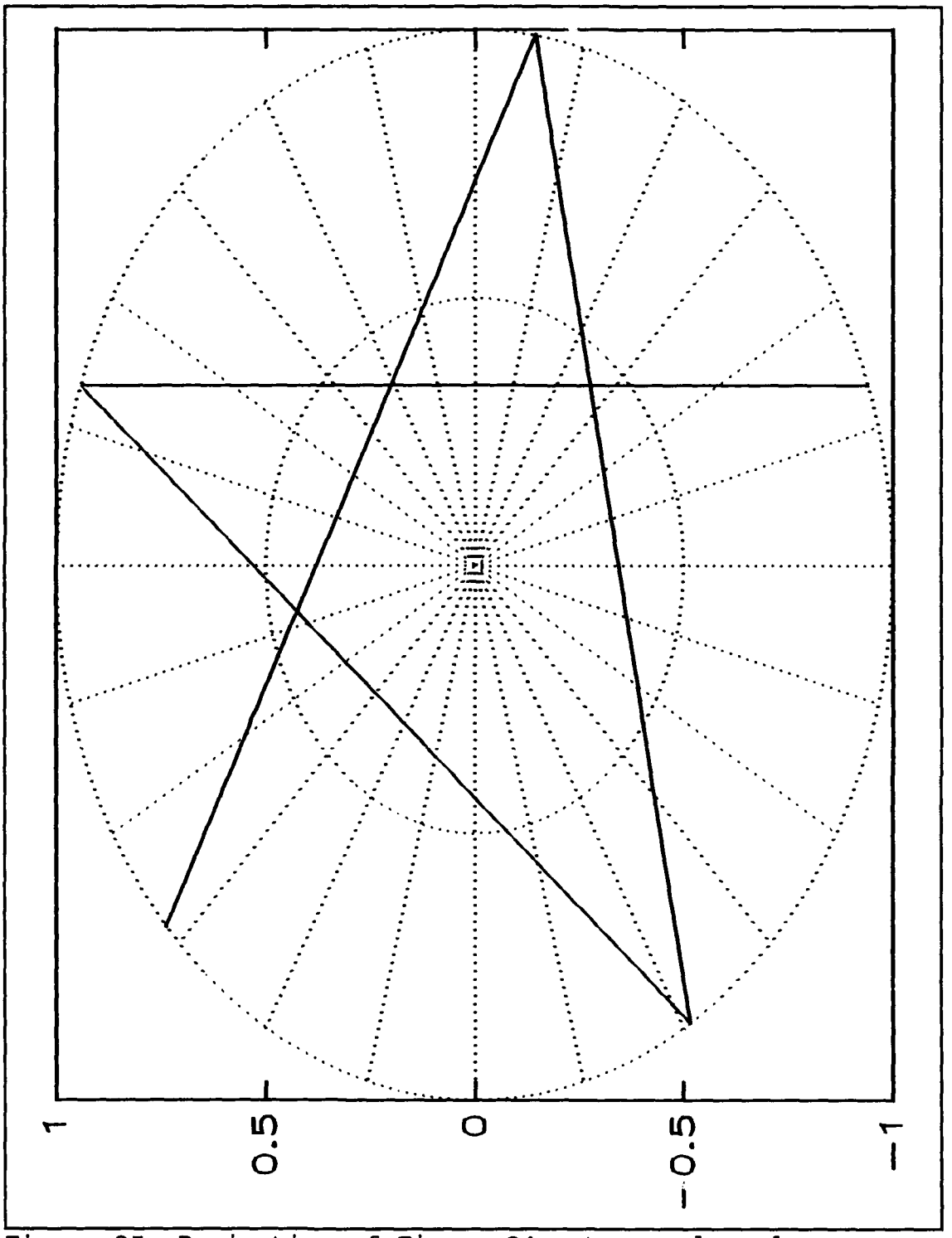

Figure 25: Projection of Figure 24 onto a polar plane.

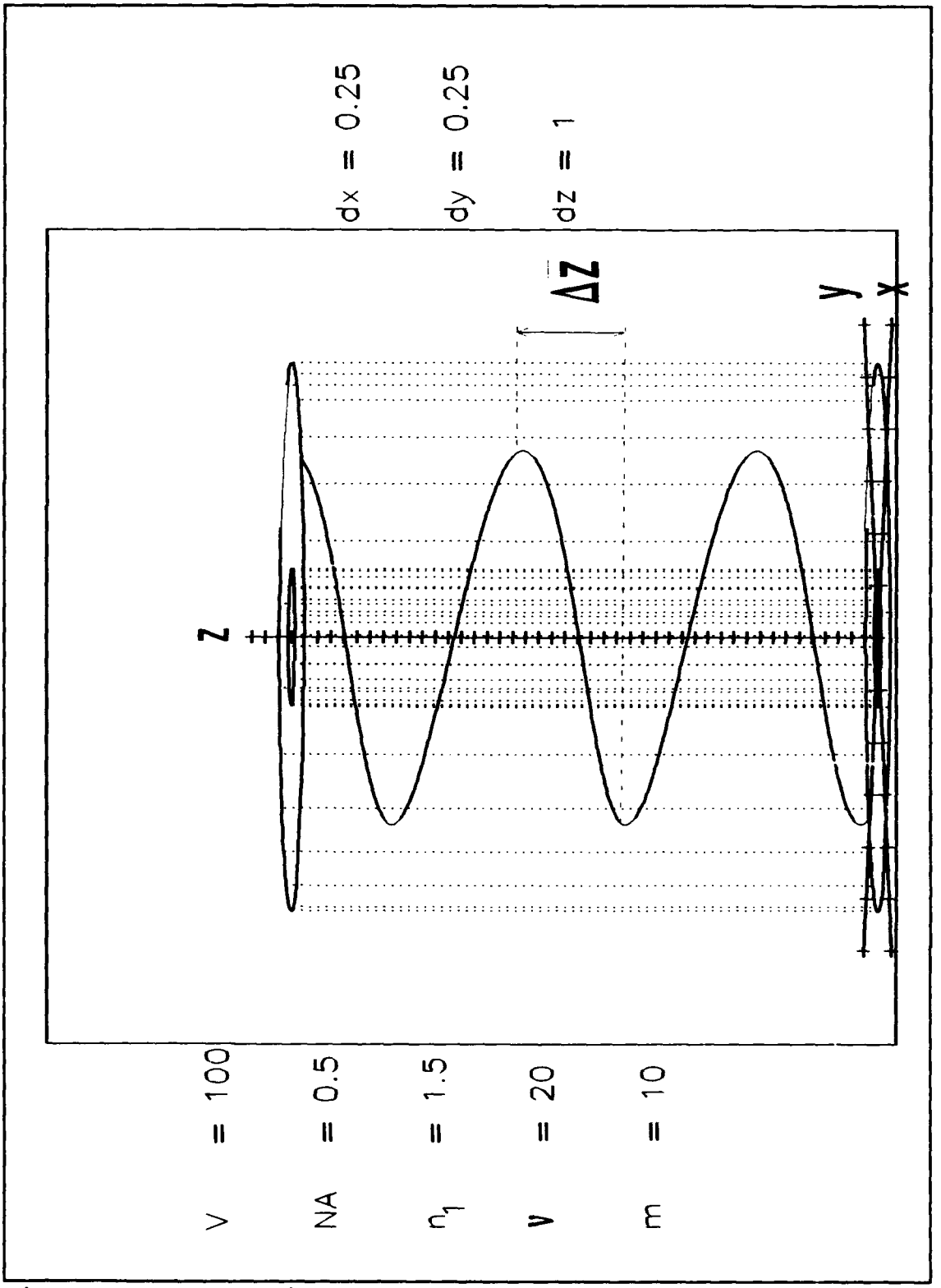

Figure 26: Ray trajectory for α=2.

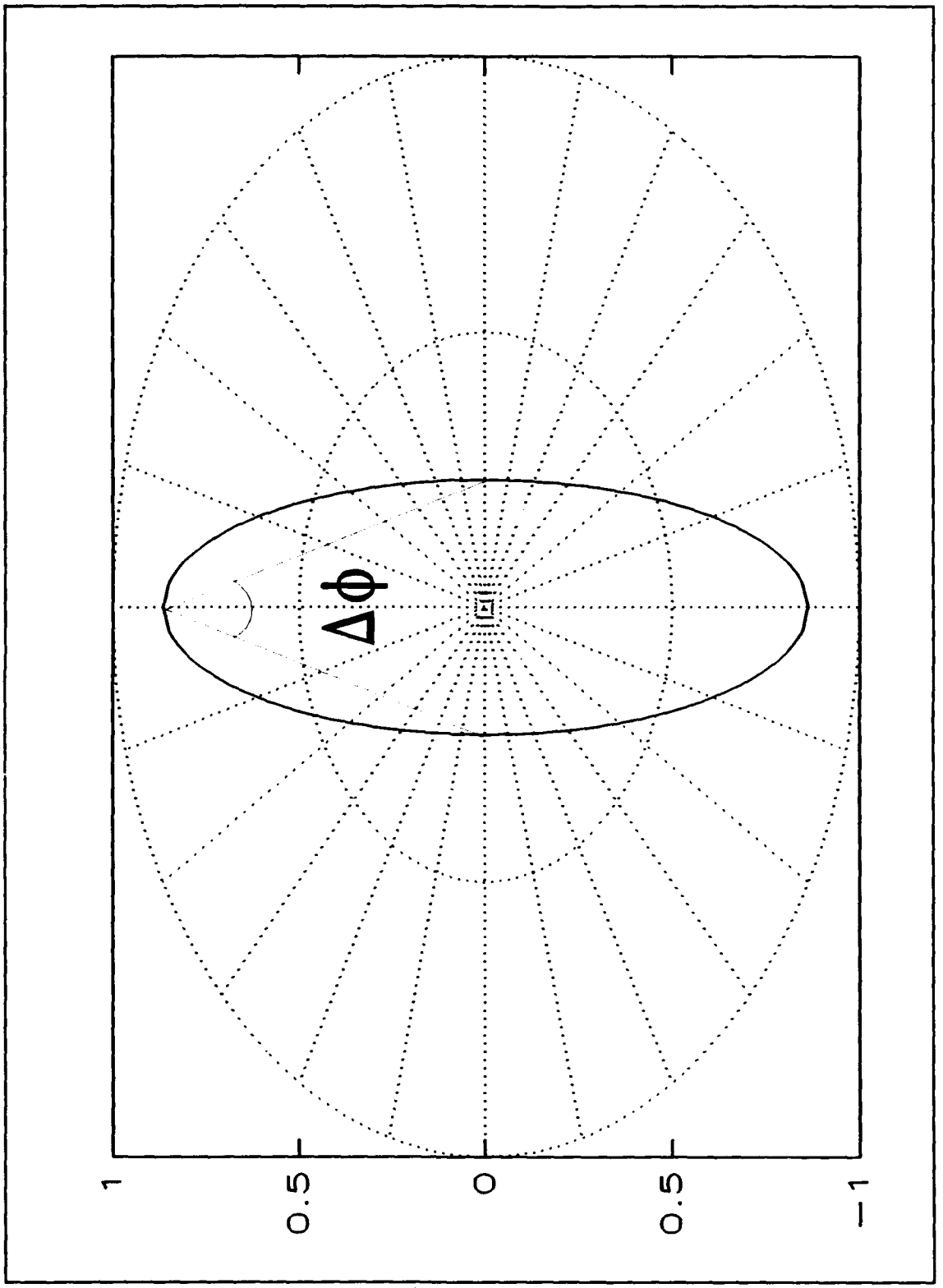

Figure 27: Axial view of Figure 26.

m	ν	ν_{max}	m_{max}	$\bar{r}_1$	$\bar{r}_2$	$\Delta\bar{z}$	$\Delta\phi$ [rad]
2	20	50	2	0.327	0.610	9.170	0.984
6	20	50	4	0.289	0.689	9.126	0.794
8	20	50	6	0.265	0.754	9.083	0.675
10	20	50	8	0.246	0.812	9.039	0.588
15	20	50	15	0.204	0.978	8.885	0.411
10	4	50	23	0.057	0.690	9.170	0.164
10	8	50	21	0.108	0.740	9.126	0.289
10	12	50	19	0.152	0.785	9.083	0.382
10	16	50	17	0.193	0.826	9.039	0.459

Table 2: Variations of fiber parameters for α=2.

(3-15) and (3-17) that with m fixed any increase in ν must be compensated by a decrease in β. The interpretation of as the z component of the propagation vector $\vec{k}(r)$ (see Figure 2) then clarifies the slight decrease in Δz. In the upper half of the table, ν is held fixed while m varies between 2 and 10.

ν_{max}	ν	m_{max}	m	$\bar{r}_1$	$\bar{r}_2$	$\Delta\bar{z}$	$\Delta\phi$ [rad]
99	2	30	10	0.057	0.999	17.261	0.114
99	10	26	10	0.217	0.999	12.581	0.437
99	18	23	10	0.316	0.999	9.845	0.643
99	20	22	5	0.472	0.999	12.384	0.984
99	20	22	15	0.263	0.999	7.386	0.532
99	20	22	20	0.217	1	6.069	0.437

Table 3: Variations of fiber parameters for α=10000.

ν_{max}	ν	m_{max}	m	$\bar{r}_1$	$\bar{r}_2$	$\Delta\bar{z}$	$\Delta\phi$ [rad]
68	5	26	5	0.139	0.705	14.075	0.396
68	30	15	5	0.425	0.850	8.129	1.030
68	45	8	5	0.512	0.902	6.745	1.176
68	5	26	25	0.052	0.986	7.083	0.105
68	5	26	15	0.073	0.879	9.118	0.166
68	5	26	5	0.139	0.705	14.075	0.396

Table 4: Variations of fiber parameters for α=6.

According to Figure 2, it is clear that as m increases, β decreases, and as such, Δz should decrease. This pattern is again evident from the table. Referring back to the relation between β and $\epsilon(\beta)$, given by (3-17), and the discussion of the dependence of turning points on $\epsilon(\beta)$ in Chapter III, it is readily confirmed that the turning points will move together as m increases (see Figure 6). It follows from (6-3) that if $\bar{r}_1 \rightarrow \bar{r}_1 + \Delta\bar{r}_1$ and $\bar{r}_2 \rightarrow \bar{r}_2 - \Delta\bar{r}_2$, that $\Delta\phi$ will decrease, an evident pattern in the table.

It is noted that Table 3 was derived under the same conditions as the step index skew rays for Table 6 in Appendix E, except that here, α is not infinite but very big. The fact that the results of those two tables are approximately the same, demonstrates that the arbitrary α three dimensional analysis presented in this chapter is in agreement with the step index analysis.

D. FINAL REMARKS

In this chapter, ray trajectories were established for the most general case of Chapter III. Although many numerical calculations have to be done, the model is still fairly simple. Also, the demonstration that trajectory dependence on the mode numbers agrees with theoretical expectations, is one more sign of the validity of the model.

VII. QUASI ANALYTIC SOLUTION FOR SKEW RAYS WITH α=2

A. INTRODUCTORY REMARKS

In this chapter, the three-dimensional skew ray analysis will be examined for the special case α=2. This case has special significance for telecommunications applications. It is for this profile, the so called parabolic profile, that multimode fibers exhibit an approximate minimum in modal dispersion [Ref. 1]. It turns out that the integrals describing the ray trajectories (see (6-1) and (6-2)) and radial mode number (see (3-15) with f(r)=0) can be evaluated analytically for the case α=2. Although numerical integration is no longer needed, the general relationship between m, $\epsilon(\beta)$, $\bar{r}_1$ and $\bar{r}_2$ is too complex to be established without the assistance of a numerical root finding algorithm.

B. ANALYSIS

For α=2, (3-27) becomes

$$\nu_{max}=\frac{V}{2}. \tag{7-1}$$

The radial mode number can be found by setting $\bar{x}=\bar{r}^2$ and f(r)=0 into (3-15), yielding

$$m=\frac{V}{\pi}\int_{\bar{x}_1}^{\bar{x}}\frac{1}{2\bar{x}}\sqrt{\epsilon(\beta)\bar{x}-(\frac{\nu}{V})^2-\bar{x}^2}\,dx, \tag{7-2}$$

where the turning points are (see (3-19)) given by

$$\bar{x}_{1,2}=\frac{\epsilon(\beta)\pm\sqrt{\epsilon^2(\beta)-4(\frac{\nu}{V})^2}}{2}. \tag{7-3}$$

After using [Ref. 18]

$$\int\sqrt{ax^2+bx+c}\,\frac{dx}{x}=-\frac{\sqrt{ax^2+bx+c}}{x}+\frac{b}{2}\int\frac{dx}{\sqrt{ax^2+bx+c}}+c\int\frac{dx}{x\sqrt{ax^2+bx+c}}, \tag{7-4}$$

$$\int\frac{dx}{\sqrt{ax^2+bx+c}}=-\frac{1}{\sqrt{-a}}\sin^{-1}(\frac{2ax+b}{b^2-4ac}), \tag{7-5}$$

and

$$\int\frac{dx}{x\sqrt{ax^2+bx+c}}=\frac{1}{\sqrt{-c}}\sin^{-1}(\frac{bx+2c}{|x|\sqrt{b^2-4ac}}) \tag{7-6}$$

in (7-2), it follows that

$$m=\frac{V}{2\pi}[-\frac{\epsilon(\beta)}{2}\sin^{-1}(\frac{-2\bar{x}+\epsilon(\beta)}{\sqrt{\epsilon^2(\beta)-4(\frac{\nu}{V})^2}})-\frac{\nu}{V}\sin^{-1}(\frac{\epsilon(\beta)\bar{x}-2(\frac{\nu}{V})^2}{\bar{x}\sqrt{\epsilon^2(\beta)-4(\frac{\nu}{V})^2}})]_{\bar{x}_1}^{\bar{x}}, \tag{7-7}$$

where the limits are defined by (7-3). Equation (7-7) is not analytically invertible so it is necessary to have the computer find $\epsilon(\beta)$ using the root searching algorithm shown in

Figure 19. Similarly, m_{max} can be found after setting $\epsilon(\beta)=1$ in (7-7) and directly evaluating the expression.

In order to obtain the trajectory for $\alpha=2$, (6-1) becomes

$$\bar{z}(\bar{x}) = \frac{\sqrt{n_1^2 - NA^2\epsilon(\beta)}}{2NA} \int_{\bar{x}_1}^{\bar{x}} \frac{dx}{\sqrt{-\bar{x} + \epsilon(\beta)\bar{x} - (\frac{\nu}{V})^2}}, \qquad (7\text{-}8)$$

which can be evaluated using (7-5) and leads to

$$\bar{z}(\bar{x}) = \frac{\sqrt{n_1^2 - NA^2\epsilon(\beta)}}{2NA} \left[-\sin^{-1}\left(\frac{-2\bar{x} + \epsilon(\beta)}{\sqrt{\epsilon^2(\beta) - (\frac{\nu}{V})^2}} \right) \right]_{\bar{x}_1}^{\bar{x}}, \qquad (7\text{-}9)$$

where $\bar{x} \epsilon [\bar{x}_1, \bar{x}_2]$. The limits are given in (7-3).

For $\phi(\bar{x})$, (6-2) for $\alpha=2$ becomes

$$\phi(\bar{x}) = -\frac{\nu}{2V} \int_{\bar{x}_1}^{\bar{x}} \frac{dx}{\bar{x}\sqrt{-\bar{x} + \epsilon(\beta)\bar{x} - (\frac{\nu}{V})^2}}, \qquad (7\text{-}10)$$

and by using (7-6), (7-10) becomes

$$\phi(\bar{x}) = -\frac{1}{2} \left[\sin^{-1}\left(\frac{\epsilon(\beta)\bar{x} - 2(\frac{\nu}{V})^2}{\bar{x}\sqrt{\epsilon^2(\beta) - 4(\frac{\nu}{V})^2}} \right) \right]_{\bar{x}_1}^{\bar{x}}, \qquad (7\text{-}11)$$

where $\bar{x} \epsilon [\bar{x}_1, \bar{x}_2]$. It is easy to show that substitution of (7-3) into (7-11) leads to

$$\phi(\bar{x}_1) = 0 \qquad (7\text{-}12)$$

and

$$\phi(\bar{x}_2) = \frac{\pi}{2}, \qquad (7\text{-}13)$$

respectively. After four applications of (7-11), $\phi(\bar{x})=2\pi$, which proves the periodicity of ray trajectories with $\alpha=2$, in agreement with References 8 and 20.

Figure 28 shows a three-dimensional plot of a numerically calculated skew ray trajectory for conditions given on the Figure. Its axial view, Figure 29, demonstrates clearly that the ray trajectory on the XY plane is a closed orbit. As soon as the ray trajectory returns to the same point on the XY plane after four applications of (7-11), the z component of the ray trajectory is also forced to be periodic.

Both the numerical ray tracing program used in Chapter VI, *and the quasi analytic* ray tracing program for $\alpha=2$, were tested under the same conditions as given in Figure 28. It was determined that both programs produced exactly the same results with no greater then 0.1% discrepancy. These results lend confidence to the reliability of the models.

C. EXAMPLES

Table 5 was derived from repeated applications of (7-9) and (7-11) under optical fiber conditions consistent with V, NA, n_1 and α defined on Figure 28. The parameter $\Delta\bar{z}$ is defined on Figure 28, and $\Delta\phi$ is defined on Figure 29.

The discussion of the variation of parameters in Table 5 has already been explained with similar tables in Chapter VI.

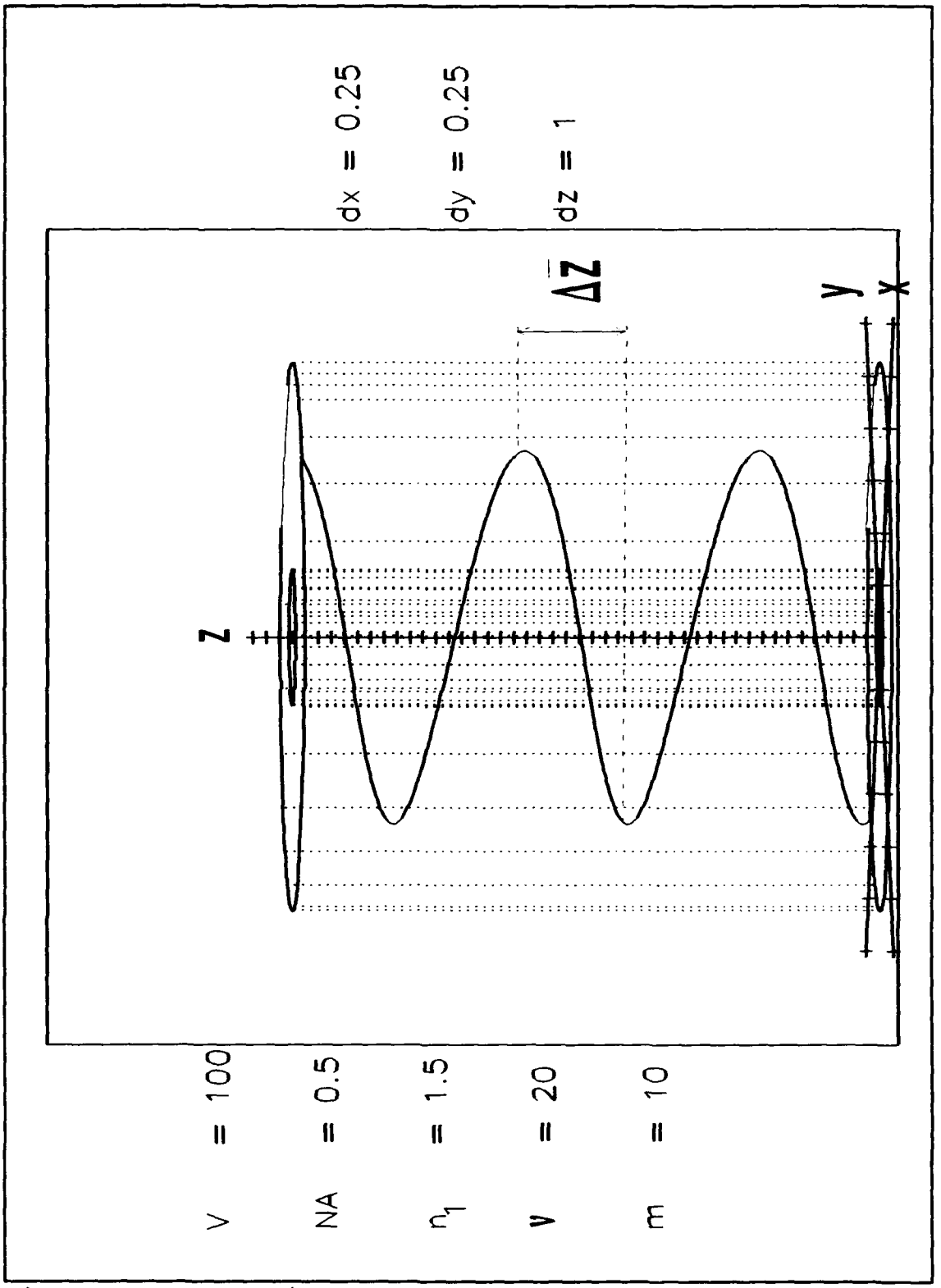

Figure 29: Ray trajectory for α=2.

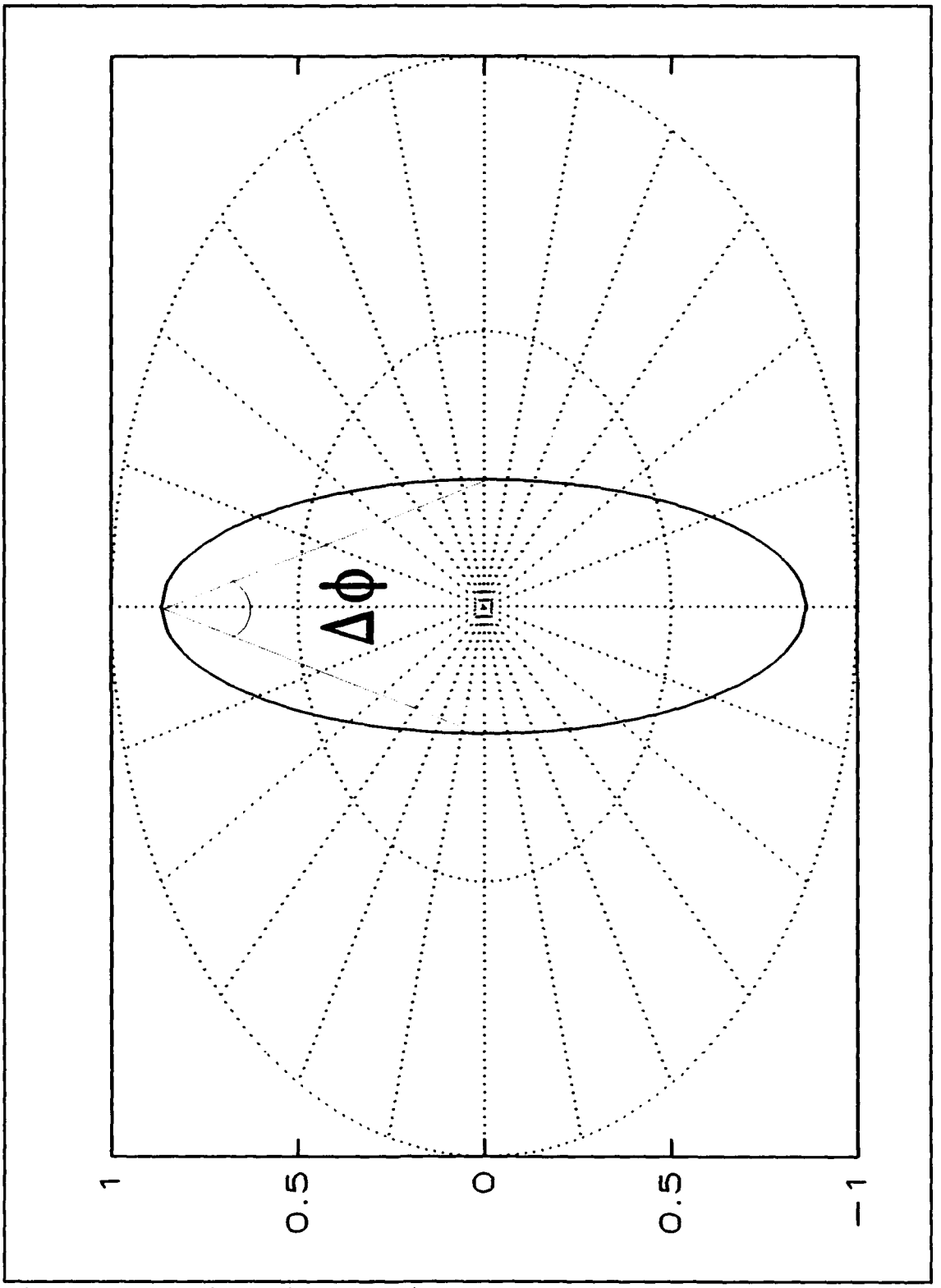

Figure 29: Axial view of Figure 28.

m	ν	ν_{max}	m_{max}	$\bar{r}_1$	$\bar{r}_2$	$\Delta\bar{z}$	$\Delta\phi$ [rad]
2	20	50	2	0.327	0.610	9.170	0.984
6	20	50	4	0.289	0.689	9.126	0.794
8	20	50	6	0.265	0.754	9.083	0.675
10	20	50	8	0.246	0.812	9.039	0.588
15	20	50	15	0.204	0.978	8.885	0.411
10	4	50	23	0.057	0.690	9.170	0.164
10	8	50	21	0.108	0.740	9.126	0.289
10	12	50	19	0.152	0.785	9.083	0.382
10	16	50	17	0.193	0.826	9.039	0.459
5	40	50	5	0.447	0.894	8.885	0.927

Table 5: Variations of fiber parameters for α=2.

It is easily checked that the parameter variations shown in the analytically generated Table 5 follow the same trends as seen in all the tables of Chapter VI.

D. FINAL REMARKS

In the previous chapter the case of α=2 was studied with the assistance of numerical integrations. It was demonstrated in Figure 27 that the trajectory actually followed a closed orbit for the specific fiber parameters. It was shown in this chapter that the result is exact and only depends on the condition that α=2. This somewhat remarkable result has been discussed in the literature. Specifically, the analogies between mechanics and optics provides the insight as the basis for this effect [Ref. 8]. It turns out that only two kinds of

potentials exist which can lead to closed orbits. First, there is the $\frac{1}{r}$ potential, applicable to celestial bodies, and second, the r^2 potential associated with harmonic oscillators [Ref. 20]. It is the harmonic oscillator potential which is the analog of the parabolic profile.

VIII. CONCLUSIONS

The two main categories that deal with optical fibers are guided-wave electromagnetic modes and ray optics. Although these approaches both describe the propagation of waves, they are not directly connected. That is because the first category relies on waveguide theory to yield mode dispersion fields; while the second category uses initial conditions to establish ray trajectories. Previously, there was no way to move from angles of approach to waveguide modes, or relate ray trajectories to fields. The model presented in Chapter III has established a general formalism for connecting waveguide modes and ray trajectories. Specific cases are examined in Chapters IV through VII.

As shown in all cases, the model relating the mode numbers is fairly simple. This and the fact that three-dimensional perspectives of ray trajectories can be easily produced, facilitates the generation of physical insight for a deeper understanding of optical fibers.

It is noted that the results in Chapter V, Chapter VI and Appendix E show that the trajectory dependence on the mode numbers agrees with theoretical expectations. The direct proof in Appendix B that shows that the evolution equations are in agreement with standard Eikonal analysis makes the model presented valid.

Finally, the connection between modes and rays can ultimately lead into new methods in treating waveguide dispersion and bending losses, but this is a matter for further research.

APPENDIX A. CONCEPTUAL FLOWCHART

The flowchart shown in Figure 30 summarizes the main steps in the development leading to mode specific trajectories.

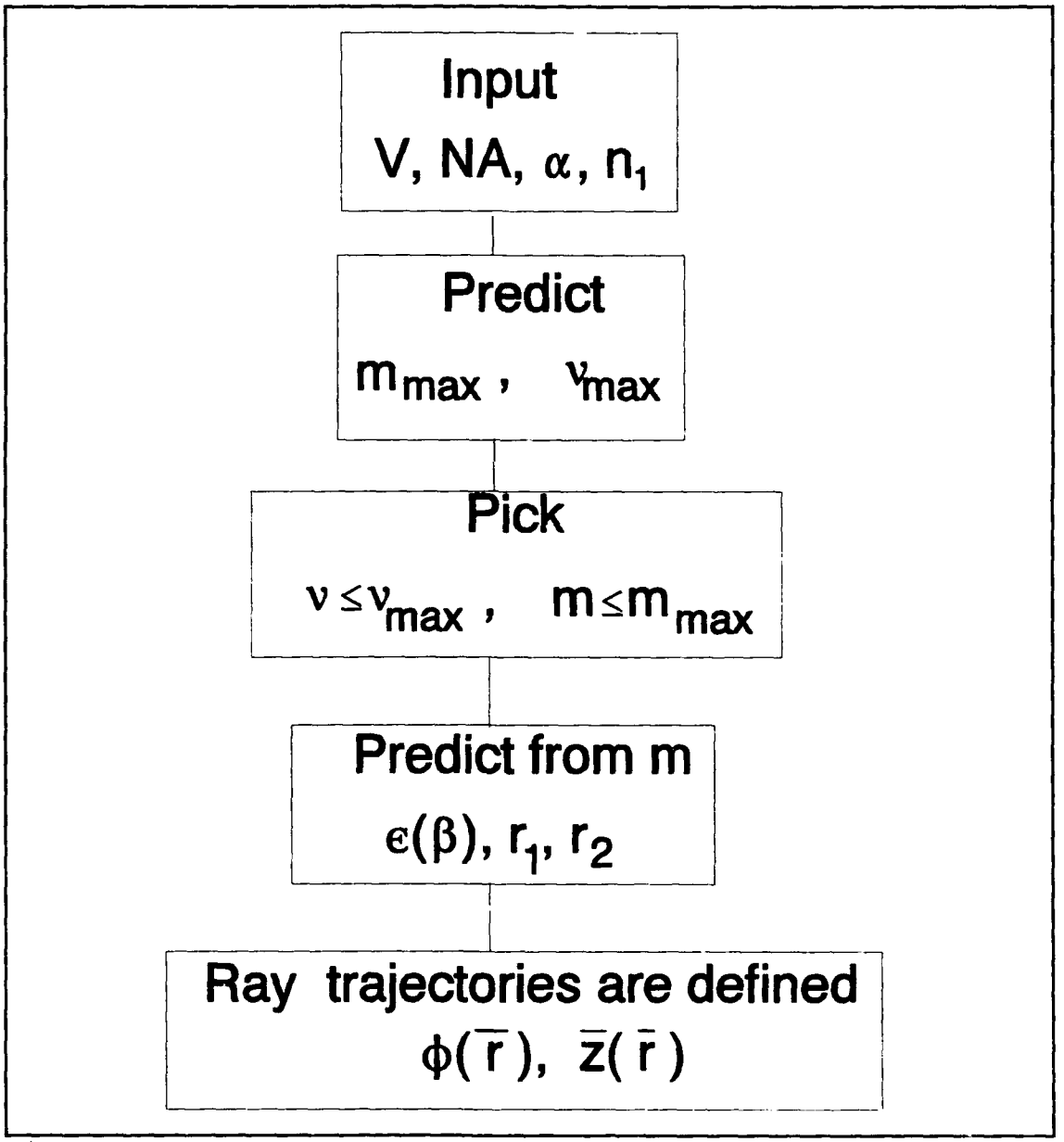

Figure 30: Conceptual flowchart.

APPENDIX B. A COMPARISON TO EIKONAL ANALYSIS

The proposed evolution equations that describe the ray trajectories in the fiber optic according to the Eikonal approach [Ref. 9] are

$$\frac{dr}{dz} = \left(\frac{n^2(r)}{E} - \frac{\ell^2}{r^2} - 1 \right)^{\frac{1}{2}} \tag{B-1}$$

and

$$\frac{d\phi}{dz} = \frac{\ell}{r^2}, \tag{B-2}$$

where E and ℓ are constants of the motion defined as

$$E = n(r) \frac{dz}{ds} \tag{B-3}$$

and

$$\ell = r^2 \frac{d\phi}{dz}, \tag{B-4}$$

with s being the distance of the point measured along the ray trajectory. All other parameters appearing in (B-1) through (B-4), are defined in the discussion in Chapter III and Figure 5. In the discussion to follow, we demonstrate the relation between the Eikonal constants of motion and the invariants β and ν.

Definition of dl in Figure 5 and (3-4) leads to

$$ds=dl. \tag{B-5}$$

By substituting (B-5) and (3-5) into (B-3), we have

$$E=n(r)\cos\theta, \tag{B-6}$$

which through combinations of (2-10) and (3-2) becomes

$$E=\frac{\beta}{k}, \tag{B-7}$$

which relates the phase constant β to the Eikonal constant E.

Also, substitution of (3-5) and (3-7) into (B-4) gives

$$\ell=r\frac{\sin\theta\sin\xi}{\cos\theta}, \tag{B-8}$$

which when combined with (2-8), (2-10), (3-1) and (3-2) leads to

$$\ell=-\frac{\nu}{\beta}. \tag{B-9}$$

Equation (B-9) relates the azimuthal mode number ν and the phase constant β to the Eikonal constant ℓ.

Finally, substitution of (B-7) and (B-9) into (B-1) leads to

$$\frac{dz}{dr}=\frac{\beta}{\sqrt{k^2n^2(r)-\beta^2-(\frac{\nu}{r})^2}}=\frac{\beta}{k_r}, \tag{B-10}$$

and substitution of (B-9) and (B-10) into (B-2) in the form

$$\frac{dr/dz}{d\phi/dz} \tag{B-11}$$

leads to

$$r\frac{d\phi}{dr} = -\frac{\nu}{r}\frac{1}{\sqrt{k^2n^2(r) - \beta^2 - (\frac{\nu}{r})^2}}. \qquad \text{(B-12)}$$

Since (B-10) is equivalent to (3-28), and (B-12) is equivalent to (3-33), which are the basic evolution equations of the proposed analysis, there is an exact agreement between the analysis presented and the Eikonal analysis. Nevertheless, the treatment presented in this thesis connects Eikonal invariants to quantized wave mode numbers.

APPENDIX C. SYMBOL TABLE

NOTATION	EXPLANATION
V	V parameter
a	core radius
n_1	core index
n_2	cladding index
NA	numerical aperture
α	power profile parameter
k	vacuum propagation constant ($\frac{\omega}{c}$)
k_1	core propagation constant ($\frac{\omega n_1}{c}$)
k_2	cladding propagation constant ($\frac{\omega n_2}{c}$)
λ	vacuum propagation wavelength ($2\pi/k$)
ν	azimuthal mode number
m	radial mode number
r, ϕ, z	coordinate system defining ray location ($\vec{k}_1$)
θ, ξ	angles which define ray orientation ($\vec{k}_1$)
θ_c	critical angle
β	phase constant
$\epsilon(\beta)$	normalized phase constant

r_{min}, r_{max}, r_1, r_2	extremes in radial excursions
Λ	trajectory period
$F(\alpha)$	normalization integral
Δ	index difference $\frac{n_1^2-n_2^2}{2n_1^2}$
$\bar{r}, \bar{z}$	$\frac{r}{a}$, $\frac{z}{a}$
ℓ, E	Eikonal invariants

APPENDIX D. PROPERTIES OF F(α)

In this Appendix we examine F(α) given by (4-8), that is,

$$F(\alpha)=\int_0^1\sqrt{1-u^{\alpha}}\,du. \tag{D-1}$$

As discussed in Chapter IV, F(α) cannot be solved analytically for all values of α. However, for some cases, solutions of F(α) can be obtained exactly.

It is easy to show that

$$F(0)=0 \tag{D-2}$$

and

$$F(\infty)=1. \tag{D-3}$$

Also, by using [Ref. 18]

$$\int\sqrt{ax+b}\,dx=\frac{2\sqrt{(ax+b)^3}}{3a} \tag{D-4}$$

and

$$\int\sqrt{a^2-x^2}\,dx=\frac{x\sqrt{a^2-x^2}}{2}+\frac{a^2}{2}\sin^{-1}\left(\frac{x}{a}\right), \tag{D-5}$$

(D-1) takes the form

$$F(1)=\frac{2}{3} \tag{D-6}$$

and

$$F(2)=\frac{\pi}{4}, \tag{D-7}$$

respectively.

Since $u^{\alpha}\equiv e^{\alpha lnu}$, then for $\alpha<1$

$$u^{\alpha}=1+\alpha lnu+\frac{(\alpha lnu)^2}{2!}+\frac{(\alpha lnu)^3}{3!}+\ldots\simeq 1+\alpha lnu, \tag{D-8}$$

which when substituted into (D-1) leads to

$$F_1(\alpha)\simeq\int_0^1\sqrt{\alpha lnu}\,du. \tag{D-9}$$

After integration of (D-9) [Ref. 18], we find

$$F_1(\alpha)\simeq\frac{\sqrt{\alpha\pi}}{2}, \tag{D-10}$$

for $\alpha\ll 1$.

For α much greater than one, and since $|u|<1$, we may assume that

$$\sqrt{1-u^{\alpha}}\simeq 1-\frac{u^{\alpha}}{2}. \tag{D-11}$$

Substitution of (D-11) into (D-1) and integration [Ref. 18] leads to

$$F_2(\alpha)\simeq\frac{2\alpha+1}{2\alpha+2} \tag{D-12}$$

for $\alpha\gg 1$.

Figure 8 shows a numerical calculation of $F(\alpha)$ for several values of α. Comparison with $F_1(\alpha)$ and $F_2(\alpha)$ shows that the

functions are asymptotic to $F(\alpha)$ for small α and large α, respectively.

APPENDIX E. REFERENCE 19 AS PRESENTED AT SSST 93

A Heuristic Approach to the Computation of 3D-ray Trajectories in Step Index Optical Fibers

Athanasios Nassopoulos and Ron Pieper

Electrical and Computer Engineering
Naval Postgraduate School
Monterey, CA 93943

Abstract

3D-ray trajectories in an optical fiber are derived through use of a simple correspondence principle. The ray trajectories are linked to the mode number of the exact waveguide solutions. The analysis and simulations presented will be in terms of dimensionless parameters needed to characterize the optical fiber. Specifically this includes the V-parameter, the core index of refraction, and the numerical aperture. The curves prepared are presented for allowed radial and azimuthal mode numbers and are presented in terms of dimensions which are normalized by the core radius. Although this approach is extendible to graded index fibers this development will not be presented in this report.

Introduction

Exact waveguide solutions have been derived for a select number of index of refraction profiles. Among

these exact solutions, the derivation for the step-index case commonly appears in most introductory and intermediate level optical fiber texts e.g. [1]. Despite the mathematical importance of having an exact solution for the propagation in an optical fiber, the wave solutions can be difficult to interpret physically. It is not surprising that an alternate method to treating optical fibers, the approximate Eikonal ray approach [2], which in turn is based on Fermat's extremum principle, has been repeatedly applied in order to visualize effects which occur in optical fibers [3]. For example, bending losses [4] and dispersion effects [5] in optical fibers have been treated using this approach. However, in the Eikonal approach the derived ray trajectories are not automatically related to the radial and azimuthal mode numbers.

Recently an approach based on a simple correspondence between waves and rays has been proposed as a substitute for the first order WKB analysis in producing the Eikonal-equivalent of the ray propagation equations [6]. This correspondence principle has been used to qualitatively demonstrate that there is a direct association between the exact wave modes and the allowed ray trajectories in an optical fiber.

Background

Starting from the Hemholtz equation which is the phasor form of the wave equation in linear, isotropic source-free homogeneous media, we have

$$[\nabla^2+k^2(\bar{r})]\bar{E}=0, \qquad \text{(E-1)}$$

where k($\bar{r}$) is the wave number and $\bar{E}$ is the electric field. It is noted that this equation is only approximately valid in a graded index fiber. Consistent with the form given in (E-1) we assumed that

$$k^2(r)=n^2(r)k^2=k_r^2+k_\phi^2+k_z^2, \qquad \text{(E-2)}$$

where k is the vacuum wave number, n(r) is the index of refraction, and r, ϕ and z are cylindrical coordinates needed to describe points in the fiber. Following a standard procedure [1] in waveguide analysis we assume that

$$E_z(r)=F(r)e^{j\nu\phi}e^{-j\beta z} \qquad \text{(E-3)}$$

where ν, the azimuthal mode number, is forced to be an integer due to periodic boundary conditions.

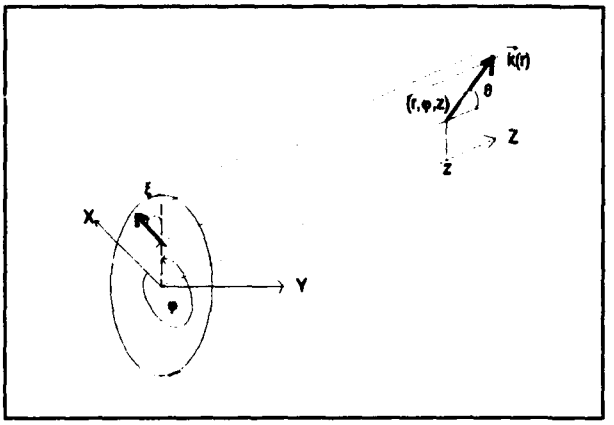

Figure 31: Geometry of the problem

β is the phase constant of the wave guide. F(r) is the radial solution to (E-1). In a step index fiber the exact waveguide solution for F(r) can be expressed on terms of Bessel Functions [1,3].

Using a simple correspondence rule, $\nabla \rightarrow j\bar{k}$, it is easily shown [6] that

$$k_\phi = -\frac{\nu}{r} \qquad \text{(E-4)}$$

$$k_z = \beta. \qquad \text{(E-5)}$$

A condition of phase synchronization [1] on the radial part of the wave vector results in an approximate integral expansion

$$m \approx \frac{1}{\pi}\int_{r_1}^{r_2}\sqrt{k^2(r)-\beta^2-(\frac{\nu}{r})^2}\,dr \qquad \text{(E-6)}$$

where the radial mode number m takes on positive integer values.

Equations (E-4), (E-5) and (E-6) become the basis for the three dimensional ray modeling that will be the focus of the discussion that follows. It is noted that the components (k_r, k_ϕ, k_z) will describe the direction of the ray and that (r, ϕ, z) locate the ray. For purposes of analysis the geometrical relationships are more carefully defined in the next section.

Geometry of the problem

With reference to Fig. 31 the orientation of the wave vector is defined in terms of θ and ξ. It follows that

$$k_\phi = k(r)\sin\theta\,\sin\xi \qquad \text{(E-7)}$$

$$k_z = k(r)\cos\theta \qquad \text{(E-8)}$$

$$k_r = k(r)\sin\theta\,\cos\xi. \qquad \text{(E-9)}$$

Letting $d\bar{l}$ represent the line variation in the ray location defined by

$$\vec{dl} = dz\,\hat{e}_z + dr\,\hat{e}_r + r\,d\phi\,\hat{e}_\phi \qquad \text{(E-10)}$$

and that the incremental components $d\phi$, dr, dz are tangential to (E-7), (E-8) and (E-9) respectively, it follows

$$dz = dl\cos\theta \qquad \text{(E-11)}$$

$$dr = dl\sin\theta\cos\xi \qquad \text{(E-12)}$$

$$r\,d\phi = dl\sin\theta\sin\xi. \qquad \text{(E-13)}$$

Through combinations of (E-7)-(E-13) the initial form of the trajectory equations becomes

$$\frac{dz}{dr} = \frac{k_z}{k_r} = \frac{\beta}{k_r} = \frac{ctn\theta}{\cos\xi} \qquad \text{(E-14)}$$

$$r\frac{d\phi}{dr} = \frac{k_\phi}{k_r} = \frac{-\frac{\nu}{r}}{\sqrt{k^2 n^2(r) - \beta^2 - (\frac{\nu}{r})^2}} = \tan\xi. \qquad \text{(E-15)}$$

The evolution equations (E-14) and (E-15), that describe the ray trajectories, can be shown to be equivalent to the Eikonal solution [7]. Because of the 3D emphasis in this report we have chosen to concentrate on skew rays ($\nu \neq 0$) instead of the less interesting meridional rays ($\nu = 0$).

Modeling Analysis. Step Index case

We follow the usual step index notation $n(r) = n_1$ for $r \leq a$ and $n(r) = n_2$ for $r > a$.On Fig. 32 the sum of the two terms in (E-6), $k^2n_1^2 - (\nu/r)^2$, is shown plotted versus r. The condition that the integration (E-6) must remain positive would indicate that the hatched region in Fig. 32 defines the allowed extremities of the possible ray trajectories. It therefore follows that

$$m = \frac{1}{\pi}\int_{r_{min}}^{a}\sqrt{k^2n_1^2 - \beta^2 - (\frac{\nu}{r})^2}\,dr. \qquad \text{(E-16)}$$

Specification of a radial number m and the azimuthal mode numbers will dictate a specific phase constant $\beta_{\nu m}$ which are ordered [1] by convention

$$k_1^2 \geq \beta_{\nu m} > \beta_{\nu\, m+1} > \ldots \beta_{\nu\, mmax} \geq k_2^2 \qquad \text{(E-17)}$$

where the upper and lower bounds on $\beta_{\nu m}$ are predictable from a combination of wave and ray analysis [1].

The turning point equation for r_{min} is obtained by setting the integrand in (E-16) to zero

$$k^2n_1^2 - \beta_{\nu m}^2 - (\frac{\nu}{r_{min}})^2 = 0. \qquad \text{(E-18)}$$

The maximum allowed ν is determined by setting $\beta_{\nu m} = n_2k_2$ and noting from Fig. 2 that $r_{min} \to a$. It follows that

$$\nu_{max} = Int\,[ka\sqrt{n_1^2 - n_2^2}] = Int\,[V] \qquad \text{(E-19)}$$

where the quantity in the brackets is the well

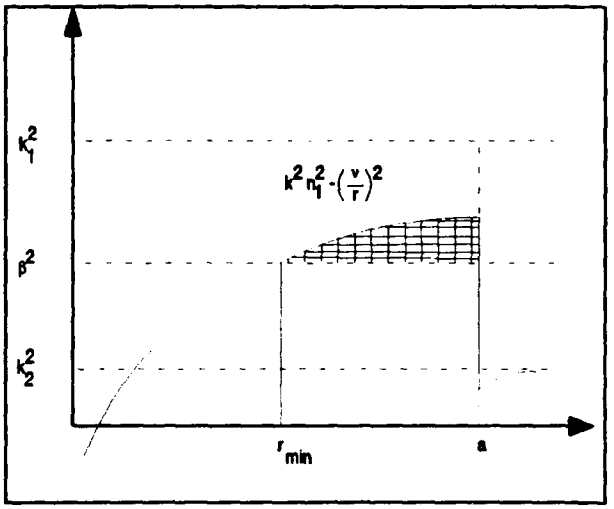

Figure 32: Step index case

known V parameter. The Int[ ] operator takes the integer part to produce a valid mode number.The general expression for r_{min} can be obtained from (E-18) as

$$r_{min}=\frac{\nu}{\sqrt{k^2n_1^2-\beta^2}}=\frac{\nu}{kn_1\sin\theta} \qquad \text{(E-20)}$$

where the second equation follows from geometric considerations. From (E-5) and (E-8), we find that (E-16) can be expressed as

$$m(\nu)=Int\,[\frac{1}{\pi}\int_{\bar{r}_{min}}^{1}\sqrt{(c\,\bar{r})^2-\nu^2}\frac{d\bar{r}}{\bar{r}}] \qquad \text{(E-21)}$$

where $C=akn_1\sin\theta$, $\bar{r}=r/a$ and $\bar{r}_{min}=r_{min}/a$. Integration leads to

$$m(\nu)=Int\,[\frac{1}{\pi}(\sqrt{C^2-\nu^2}-\nu\sec^{-1}(\frac{C}{\nu}))]. \qquad \text{(E-22)}$$

To find $m_{max}(\nu)$ it is necessary to allow C to take its maximum value. As seen from (E-5) and (E-8) this occurs for the minimum β. It follows from (E-17) that the maximum value of C is the V parameter. After direct substitution into (E-22), $m_{max}(\nu)$ satisfies

$$m_{max}(\nu)=Int\,[\frac{1}{\pi}(\sqrt{V^2-\nu^2}-\nu\sec^{-1}(\frac{V}{\nu}))]. \qquad \text{(E-23)}$$

where for $\nu=0$

$$m_{max}(0)=Int[\frac{V}{\pi}] \qquad \text{(E-24)}$$

in agreement with a mode space analysis [8].

From the set of equations (E-20) and (E-22) it can easily be shown that

$$m\pi=\nu[\sqrt{(\frac{1}{\bar{r}_{min}})^2-1}-\sec^{-1}(\frac{1}{\bar{r}_{min}})] \qquad \text{(E-25)}$$

Given that m and ν are known, the exact value of $\bar{r}_{min}$ can be found by numerically solving (E-25).

Normalized ray trajectories

In this section the normalized trajectories for rays defined by a combination of standard optical parameters (V, NA, n_1) and mode indices m and ν.

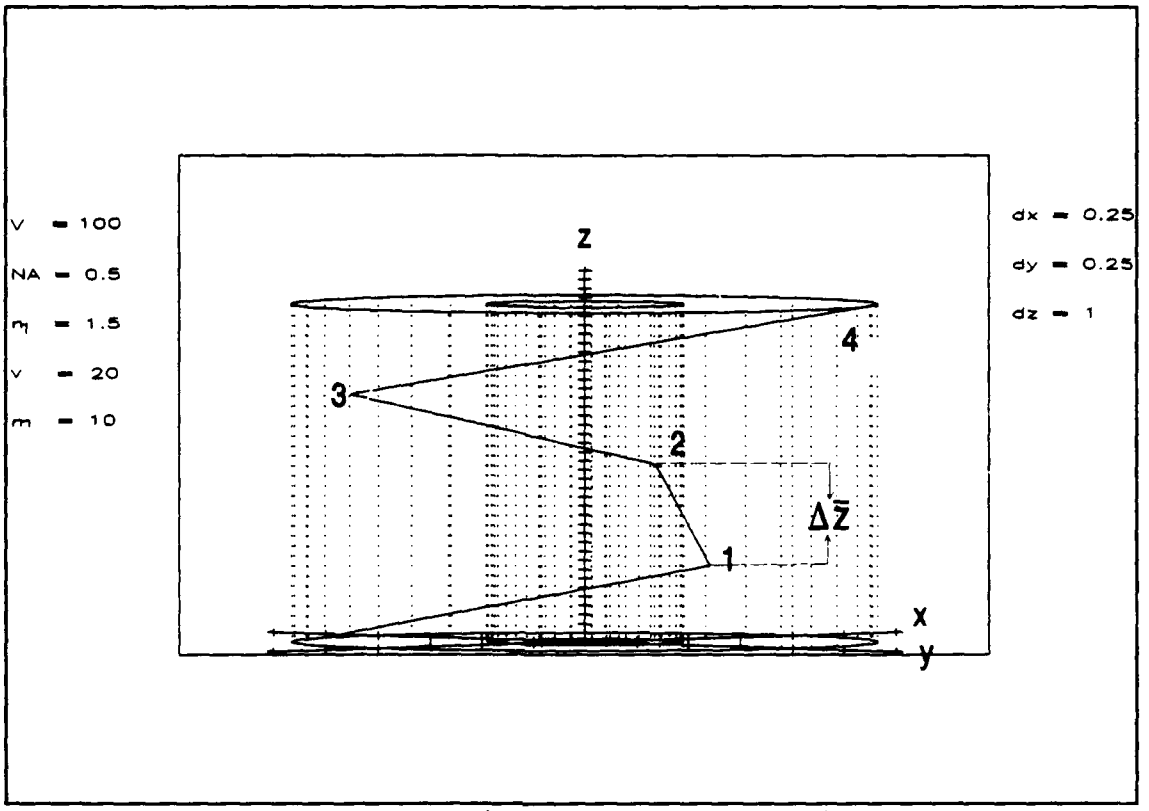

Figure 33: 3D representation showing 4 turning points

Consistent with the purpose of this report the results for meridional rays ($\nu = 0$) will be presented without significant discussion.

Starting from (E-4) and (E-7) it easy to demonstrate that

$$v = -r\, k_\phi = -r\, k\, n_1 \sin\theta \sin\xi. \qquad \text{(E-26)}$$

After substitution of (E-20) into (E-26) we have that

$$\sin\xi = -\frac{r_{min}}{r}, \qquad \text{(E-27)}$$

which is needed in the analysis to follow.

The integral form of (E-15) which is

$$\varphi(\bar{r}) = \int_{r_{min}}^{r} \tan\xi\, dr = \int_{r_{min}}^{r} \frac{\sin\xi}{\pm\sqrt{1-\sin^2\xi}} \frac{dr}{r} \qquad \text{(E-28)}$$

can be solved by substituting (E-27). Finally we have

$$\phi(\bar{r}) = \sec^{-1}\left(\frac{\bar{r}}{r_{min}}\right) \qquad \text{(E-29)}$$

which is not valid for $\nu = 0$. However from (E-15) and (E-27) $\phi(\bar{r}) = 0$ for $\nu = 0$. $z(\bar{r})$ can be found by solving the integral form of(E-14) which is

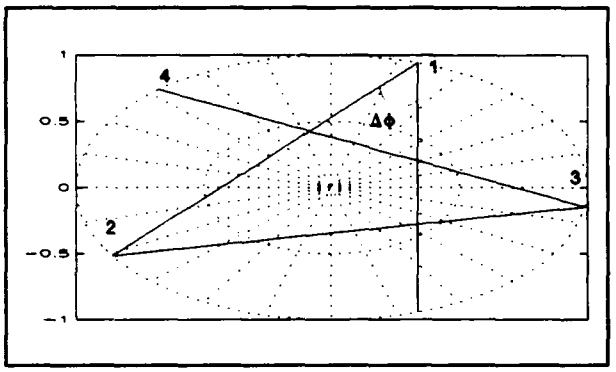

Figure 34: Projection in polar plane.

$$z(\bar{r}) = \int_{\bar{r}_{min}}^{\bar{r}} \frac{ctn\theta}{\cos\xi} d\bar{r}. \qquad \text{(E-30)}$$

With a second application of(E-27) we find

$$\bar{z}(\bar{r}) = ctn\theta\sqrt{\bar{r}^2 - \bar{r}_{min}^2}, \qquad \text{(E-31)}$$

where $\bar{z} = z/a$. The angle θ can be easily calculated from (E-20) as

$$\sin\theta = \frac{\nu}{\bar{r}_{min} V(\frac{n_1}{NA})} \qquad \text{(E-32)}$$

and where $\bar{r}_{min}$ can be obtained from (E-25). For $\nu = 0$ it can be shown that $\bar{z}(r) = \bar{r}ctn\theta$ and $\sin\theta = (mNA)/(Vn_1)$ are applicable to trajectory calculations of meridional rays.

Along with the input parameters V, NA, n_1, ν (given ν_{max} from (19)) and m (given m_{max} from (E-23)), the set of equations (E-25), (E-29), (E-31) and (E-32) determine the normalized ray trajectories of a skew ray in a step index fiber.

Discussion of results

Figure 33 shows a 3D plot of a numerically calculated skew ray trajectory for conditions given on the figure. The dense vertical lines are drawn at $\bar{r} = \bar{r}_{min}$ and the low density lines are drawn at $\bar{r} = 1.0$. Points 1, 2, 3, 4 are turning points at $\bar{r} = 1.0$. Because of the 3D perspective the normalized increment in $\Delta\bar{z}$ appears to change size. Figure 34 shows the corresponding axial view. The angle $\Delta\phi$ is defined by rays joined at the turning points.

Table 6 was derived from repeated applications under optical fiber conditions consistent with V, NA and n_1 defined on Figure 31. The trends relating variation of $\Delta\phi$ and $\Delta\bar{z}$ with ν and m are readily explained. In the upper half of the table, for fixed m, the angle $\Delta\phi$ increases with the rotational component, k_ϕ, as expected. Also, since m (E-6) is constant, β must decrease. This is manifest by $\Delta\bar{z}$ decreasing with ν. In the lower half of the table, where ν is fixed, as m increases, β, as seen from (E-6) must again drop. Again $\Delta\bar{z}$ must therefore decrease. And finally, the parallel decrease in $\Delta\phi$ (E-

Δφ[rad]	Δz̄	m	ν
0.12	17.25	10	02
0.44	12.57	10	10
0.64	09.84	10	18
0.98	12.37	05	20
0.53	07.38	15	20
0.44	06.10	20	20

Table 6: Representative variation in ray parameters with wave mode numbers.

29) can be explained geometrically as seen from figure 34 by a required decrease in r_{min}. This is apparent by noting that as the radial mode number increases with ν fixed the phase constant β should, as seen from (E-6) decrease. Conditions (E-5) and (E-8) then indicate θ will increase and therefore from (E-20) r_{min} will decrease.

Conclusions

The main point of this report on optical fiber ray calculations is to demonstrate the existence of a pedagogically attractive alternative to more formal methods such as WKB or Eikonal analysis. An important feature of the method presented is that it links the traditional cylindrical waveguide modenumbers for the exact solution to the ray trajectories. Because of this link the numerical implementation of the model can provide valuable physical insight for the fiber optic application areas such as sensors or lightwave telecommunications.

References

[1] Gerd Keiser, Optical Fiber Communications,McGraw Hill, New York, 1991.

[2] Ajoy Ghatak, Enakshi Sharma, and Jacintha Kompella, "Exact ray paths in bent waveguides," Applied Optics 27, 3180-3184,1988.

[3] John Gowar, Optical Communications Systems, Prentice Hall International, Englewood Cliffs, N.J., 1984.

[4] C. Winkler, J.D. Love, A.K. Ghatak, "Loss calculations in bent multimode optical waveguides," Optical and Quantum Electronics 11, 173-183, 1979.

[5] A. Ankiewich, C. Pask, "Geometric optics approach to light acceptance and propagation in graded index fibers," Optical and Quantum Electronics 9, 87-109, 1977.

[6] R.J. Pieper, "A Heuristic Approach to Fiber Optics," IEEE Transactions on Education, vol. E-30 number 2, 77-82, 1987.

[7] A. Nassopoulos, "The Three Dimensional Ray Trajectories of the WKB Optical Fiber Modes," M.S.E.E. Thesis, Naval Postgraduate School, 1993.

[8] A. Cherin, An Introduction to Optical Fibers, Mc Graw Hill, New York, 1991.

LIST OF REFERENCES

1. Gerd Keiser, *Optical Fiber Communications*, McGraw Hill, 1991.

2. E.W. Marchand, "Graded Index Lenses," *Progress in Optics*, v.11, pp.305-337, 1973.

3. A. Cherin, *An Introduction to Optical Fibers*, Mc Graw Hill, 1983.

4. T. Okoshi, *Optical Fibers*, Academic Press, 1982.

5. A. Ankiewich, C. Pask, "Geometric optics approach to light acceptance and propagation in graded index fibers," *Optical and Quantum Electronics*, v.9, pp.87-109, 1977.

6. M.V. Berry and C. Upstill, "Catastrophe Optics: Morphologies of Caustics and their Diffraction Patterns," *Progress in Optics*, v.18, pp.257-346, 1980.

7. M.S. Sodha and A.K. Ghatak, *Inhomogeneous Optical Waveguides*, Plenum Press, 1977.

8. R.J. Black and A. Ankiewicz, "Fiber Optics Analogies with Mechanics," *American Journal of Physics*, v.53, pp.554-563, 1985.

9. John Gowar, *Optical Communications Systems*, Prentice Hall International, 1984.

10. A. Sharma, "Computing Optical Path Length in Gradient Index Media: a Fast and Accurate Method," *Applied Optics*, v.24, pp.4367-4370, 1985.

11. A. Sharma and A.K. Ghatak, "Ray Tracing in Gradient-Index Lenses: Computation of Ray-Surface intersection," *Applied Optics*, v.25, pp.3409-3412, 1986.

12. A. Sharma, D. Vizia Kumar, and A.K. Ghatak, "Tracing Rays Through Graded Index Media: a New Method," *Applied Optics*, v.21, pp.984-987, 1982.

13. Ajoy Ghatak, Enakshi Sharma, and Jacintha Kompella, "Exact ray paths in bent waveguides," *Applied Optics*, v.27, pp.3180-3184, 1988.

14. S. Cornbleet, *Microwave and Optical Ray Geometry*, John Wiley and Sons, 1984.

15. C. Winkler, J.D. Love, A.K. Ghatak, "Loss calculations in bent multimode optical waveguides," *Optical and Quantum Electronics*, v.11, pp.173-183, 1979.

16. Colin Pask, "Exact Expressions for Scalar Modal Eigenvalues and Group Delays in Power-Law Optical Fibers," *Journal of the Optical Society of America*, v.69, pp.1599-1603, 1979.

17. R.J. Pieper, "A Heuristic Approach to Fiber Optics," *IEEE Transactions on Education*, v.E-30 no.2, pp.77-82, 1987.

18. Murray R. Spiegel, *Mathematical Handbook of Formulas and Tables*, McGraw Hill, 1968.

19. A. Nassopoulos and R. Pieper "A Heuristic Approach to the Computation of 3D-Ray Trajectories in Step Index Optical Fibers," the 25th Southwestern Symposium on Systems Theory, Alabama, March 1993.

20. H. Goldstein, *Classical Mechanics*, Addison-Wesley, 1980.

INITIAL DISTRIBUTION LIST

		No. Copies
1.	Defense Technical Information Center Cameron Station Alexandria VA 22304-6145	2
2.	Library, Code 52 Naval Postgraduate School Monterey CA 93943-5002	2
3.	Chairman, Code EC Department of Electrical and Computer Engeneering Naval Postgraduate School Monterey, CA 93940-5000	1
4.	Prof. Ronald J. Pieper, Code EC/Pr Department of Electrical and Computer Engineering Naval Postgraduate School Monterey, CA 93943-5000	1
5.	Prof. Lawrence J. Ziomek, Code EC/Zm Department of Electrical and Computer Engineering Naval Postgraduate School Monterey, CA 93943-5000	1
6.	Athanasios Nassopoulos 28 Xiou St., Ag. Paraskevi Athens, 15343 Greece	1
7.	Embassy of Greece Naval Attache 2228 Massachusetts Ave., N.W. Washington D.C., 20008	1